Insulin sensitivity and PIP_3 turnover in *Drosophila* are regulated by phosphatidylinositol 5 phosphate 4-kinase.

Sanjeev Sharma*, Swarna Mathre*^, Ramya Visvanathan*, Dhananjay Shinde* and Padinjat Raghu*%

*National Centre for Biological Sciences, TIFR-GKVK Campus, Bellary Road, Bangalore 560065, India.
^Manipal University, Madhav Nagar, Manipal 576104, Karnataka, India

% corresponding author
Tel: +91-80-23666102
E-mail: praghu@ncbs.res.in

Abstract

Phosphatidylinositol-3,4,5-trisphosphate (PIP_3) generation at the plasma membrane is a key event during activation of receptor tyrosine kinases such as the insulin receptor and is critical for normal growth and metabolism. The lipid kinases and phosphatases regulating PIP_3 levels are described but mechanisms that control their activity remains unclear. We report that in *Drosophila*, phosphatidylinositol 5 phosphate 4-kinase (PIP4K) regulates PIP_3 levels during insulin receptor activation. Depletion of PIP4K increases PIP_3 levels and augments sensitivity to insulin through enhanced Class I phosphoinositide 3-kinase (PI3K) activity. Plasma membrane localized PIP4K was sufficient to control PIP_3 levels. Animals lacking PIP4K show enhanced insulin dependent phenotypes *in vivo* and show resistance to the metabolic consequences of a high-sugar diet. Thus, PIP4K is required for normal metabolism and development. Our work defines PIP4Ks as regulators of receptor tyrosine kinase signalling with implications for growth factor dependent processes including tumour growth, T-cell activation and metabolism.

Introduction

Lipid kinases that can phosphorylate selected positions on the inositol head group of phosphatidylinositol (PI), generate second messengers that regulate multiple processes in eukaryotic cells. The generation of phosphatidylinositol 3,4,5-trisphosphate (PIP_3) through the action of Class I PI3K following growth factor receptor (e.g Insulin receptor) stimulation, is a widespread signalling reaction (Hawkins et al., 2006) that regulates normal growth and development (Engelman et al., 2006). The role of Class I PI3K activation in response to insulin receptor signalling is evolutionarily conserved and has been widely studied in metazoan models such as the fly, worm and mammals (Barbieri et al., 2003). Robust control of the levels and the dynamics of PIP_3 turnover is essential to maintain fidelity and sensitivity of information transfer during insulin signalling. This is achieved through a number of different molecular mechanisms. The Class I PI3K enzyme is a dimer of a catalytic subunit (p110) whose activity is inhibited under unstimulated conditions by the regulatory subunit (p85/50/55/60). Upstream receptor activation and subsequent binding to p-Tyr residues on the receptor and adaptor proteins relieves this inhibition. In addition, lipid phosphatases are also important in controlling PIP_3 levels at the plasma membrane. PTEN, a 3-phosphatase, hydrolyzes PIP_3 to produce $PI(4,5)P_2$ (McConnachie et al., 2003) while SHIP2 is a 5-phosphate that generates $PI(3,4)P_2$ from PIP_3 (Pesesse et al., 1998). It is well documented that mutations in genes encoding any of these enzymes can be oncogenic or result in metabolic syndromes. Loss of function in PTEN or gain of function in Class I PI3K genes results in tumour development (Luo et al., 2003) while loss of SHIP2 results in altered insulin sensitivity in mammals (Clément et al., 2001; Kaisaki et al., 2004). Thus, the control of receptor-activated PIP_3 levels is vital to the regulation of events that direct cell growth and metabolism.

Class I PI3K enzymes utilize phosphatidylinositol 4,5-bisphosphate [$PI(4,5)P_2$] as substrate to generate PIP_3. In animal cells, the major route of $PI(4,5)P_2$ synthesis is the action of phosphatidylinositol 4 phosphate 5-kinase (PIP5K), enzymes that use phosphatidylinositol 4-phosphate (PI4P) as substrate and phosphorylate position 5 of the inositol headgroup (Stephens et al., 1991). More recently, Cantley and colleagues have described a distinct class of lipid kinases, the phosphatidylinositol 5 phosphate 4-kinases (PIP4K), enzymes that utilize phosphatidylinositol 5-phosphate (PI5P) as substrate and phosphorylate position 4 to generate $PI(4,5)P_2$ (Rameh et al., 1997). Loss of PIP4Ks does not result in a drop in the mass of total cellular $PI(4,5)P_2$ but the levels of its preferred substrate, PI5P are elevated [(Gupta et al., 2013),

reviewed in (Kolay et al., 2016)]. In mammalian cells, three isoforms of PIP4Ks occur, viz. PIP4K2A, PIP4K2B and PIP4K2C. The phenotypes of mouse knockouts in each of these genes suggest a role for PIP4Ks in regulating receptor tyrosine kinase and PI3K signaling; deletion of PIP4K2A and PIP4K2B is able to slow tumor growth in p53-/- mice (Emerling et al., 2013); depletion of PIP4K2C results in excessive T-cell activation (Shim et al., 2016) and loss of PIP4K2B in mice results in hyper-responsiveness to insulin and a progressive loss of body weight in adults (Lamia et al., 2004). Previous studies have linked PIP4K2B to insulin and PI3K signalling. Overexpression of PIP4K2B in CHO-IR cells (expressing extremely low levels of endogenous PIP4K2B) results in reduced PIP_3 production following insulin stimulation (Carricaburu et al., 2003). Similarly, in U2OS cells, acute doxycycline-induced overexpression of PIP4K2A reduces AKT activation seen on insulin stimulation although changes in PIP_3 levels were not reported under these conditions (Jones et al., 2013). By contrast, a recent study has reported that in immortalized B-cells that carry a deletion of PIP4K2A, there is a reduction in PIP_3 levels following insulin stimulation (Bulley et al., 2016). Thus, although there are multiple lines of evidence suggesting a link between PIP4K and Class I PI3K signaling during insulin stimulation, the impact of the PIP4K function on PIP_3 levels remains unresolved.

It has been reported that loss of the only PIP4K in *Drosophila* results in a larval growth deficit and developmental delay. These phenotypes were associated with an overall reduction in the levels of $pS6K^{T398}$ and $pAKT^{S505}$, both outputs of *m*echanistic *T*arget *O*f *R*apamycin (mTOR) signalling. The systemic growth defect in the dPIP4K mutants ($dPIP4K^{29}$) could be rescued by enhancing mTOR complex 1(TORC1) activity through pan-larval overexpression of its activator Rheb (Durán and Hall, 2012; Gupta et al., 2013). Since then it has also been shown in mice that PIP4K2C can regulate TORC1 -mediated signalling in immune cells (Shim et al., 2016). The loss of PIP4K2C was also shown to enhance TORC1 outputs in Tsc1/2 deficient MEFs during starvation (Mackey et al., 2014). mTOR signalling can transduce multiple developmental and environmental cues including growth factor signalling, amino acid and cellular ATP levels into growth responses (Wullschleger et al., 2006). However, the relationship between PIP4K function and its role in regulating TORC1 activity and Class I PI3K signaling remains unclear.

During *Drosophila* development, larval stages are accompanied by a dramatic increase in body size. Much of this growth occurs without increases in cell number but via an increase in cellular biomass that

118 occurs in polyploid larval tissues such as the salivary gland and fat body (Church and Robertson, 1966).
119 One major mechanism that drives this form of larval growth is the ongoing insulin signalling;
120 characterized by the endocrine secretion of insulin-like peptides (dILPs) from insulin-producing cells
121 (IPCs) in the larval brain and their action on peripheral tissues through the single insulin receptor in
122 flies (Brogiolo et al., 2001). Removal of insulin receptor (*dInR*) activity (Shingleton et al., 2005) or the
123 insulin receptor substrate (*chico*) (Bohni et al., 1999) results in reduced growth and delayed development
124 through multiple mechanisms. In flies, cell size in the salivary glands can be tuned by enhancing cell-
125 specific Class I PI3K-dependent PIP_3 production (Georgiev et al., 2010). In this study, we use salivary
126 glands and fat body cells of *Drosophila* larvae to study the effect of dPIP4K on insulin receptor activated,
127 Class I PI3K signalling. We find that in *Drosophila* larval salivary gland cells, loss of *dPIP4K* enhanced
128 the growth-promoting effects of overexpressing components of the insulin signalling pathway. dPIP4K
129 regulates the levels of PIP_3 and the intrinsic sensitivity to insulin at the plasma membrane. Insulin
130 signalling activity is regulated through negative feedback from TORC1 in cells (Gual et al., 2005; Kockel
131 et al., 2010). This TORC1 dependent reduction in insulin-stimulated PIP_3 production is rendered
132 ineffective in the absence of dPIP4K. Finally, we show that these cellular changes in insulin signalling
133 have consequences on circulating sugar metabolism in larvae and also their susceptibility to insulin
134 resistance on a high-sugar diet. Altogether, we demonstrate an important physiological role for dPIP4K
135 as a negative regulator of Class I PI3K signaling during insulin stimulation in *Drosophila in vivo*.
136
137
138 ## Results
139 **dPIP4K genetically interacts with the insulin receptor signalling pathway**
140 Salivary glands are endo-replicative organs in *Drosophila* larvae that are composed of large polarized
141 polyploid cells. Previously, we have demonstrated the use of this organ as a model to study changes in
142 cell size (Georgiev et al., 2010; Gupta et al., 2013). Prior studies on insulin receptor signalling have
143 revealed a role for this pathway in the autonomous control of both cell size and proliferation (Bohni et
144 al., 1999; Brogiolo et al., 2001). However, direct evidence for such regulation in salivary glands has not
145 been demonstrated. Therefore, as proof of principle, we depleted *dInR* levels through RNA interference
146 (RNAi) selectively in the salivary glands of 3rd instar larvae using the driver *AB1*Gal4. As expected, this
147 resulted in a reduction of the average size of salivary gland cells without a change in the number of cells
148 (Fig. 1A, B, C). Likewise, overexpression of *dInR* (Fig. 1D) and *chico* (Fig. 1E) selectively in the salivary

glands also results in an increase in cell size. Thus, insulin receptor signalling regulates cell size in the salivary gland.

We then compared the effect of overexpressing *dInR* in wild-type and *dPIP4K*^{29} cells. When *dInR* was over-expressed in *dPIP4K*^{29} (*AB1>dInR; dPIP4K*^{29}), we also found an increase in salivary gland cell size; but the increase in cell size elicited was significantly greater than that seen in wild-type cells (*AB1>dInR*) (Compare Fig. 1H(i) and (ii)). Similar results were seen when comparing the effect of *chico* overexpression in wild-type and *dPIP4K*^{29} cells; i.e. *chico* overexpression elicited a larger increase in cell size in *dPIP4K*^{29} compared to wild-type (compare Fig. 1I(i) and (ii)). We reasoned that if dPIP4K specifically interacted with the early, plasma membrane components of the insulin signalling cascade, then bypassing these by constitutively activating a downstream step will abolish the differences between wild-type and *dPIP4K*^{29} cells. In order to test this, we expressed a constitutively active form of Phosphoinositide-Dependent Kinase-1 (PDK1) (PDK1^{A467V}) which is normally activated by PIP_3 downstream of insulin receptor activation and regulates cell growth (Paradis et al., 1999; Rintelen et al., 2001). Expression of PDK1^{A467V} in salivary glands results in an increase in cell size (Fig. 1F) and this was also seen when PDK1^{A467V} was expressed in *dPIP4K*^{29} (Fig. 1G). However, in contrast to *dInR* and *chico* manipulations, the effect of overexpressing PDK1^{A467V} resulted in an equivalent cell size increase in wild-type and *dPIP4K*^{29} (Fig. 1J(i) and (ii)). These findings suggest that in *Drosophila* larval cells dPIP4K modulates insulin receptor signalling at a step that is likely to be prior to PDK1 activation.

PIP_3 levels are elevated in dPIP4K depleted larval tissues

An essential early event in InR signal transduction is the activation of Class I PI3K leading to the production of PIP_3 at the plasma membrane (Hawkins et al., 2006). Therefore, we measured PIP_3 levels at the plasma membrane by imaging salivary glands from wandering third instar larvae expressing a PIP_3-specific probe (GFP::PH-GRP1) (Britton et al., 2002). We observed that under basal conditions, plasma membrane PIP_3 in *dPIP4K*^{29} showed a small but significant elevation compared to wild-type cells (Fig. 2A(i)and (ii)). Similar results were observed in experiments with fat body cells, i.e. PIP_3 levels in *dPIP4K*^{29} fat body cells were elevated compared to wild type (Fig. 2B(i) and (ii)).

During larval development in *Drosophila*, nutritional cues and other signals result in the release of *Drosophila* Insulin-like peptides (dILPs) (Nässel and Broeck, 2016) that bind to and activate dInR

triggering Class I PI3K activation and PIP_3 production. The elevated PIP_3 levels observed in *dPIP4K*^{29} tissues could, therefore, result from (i) enhanced production and release of dILPs (ii) upregulation in insulin receptor levels (iii) increase in activity of insulin receptor or events downstream of receptor activation. To distinguish between these possibilities, we performed Q-PCR analysis to measure the levels of *dILP2, 3, 5* mRNAs [the levels of these are known to be transcriptionally regulated] (Brogiolo et al., 2001). We found that the transcript levels for these dILPs were not upregulated in *dPIP4K*^{29} compared to wildtype (Fig 2C). To check for enhanced dILP release, we measured the levels of dILP2 within the neurosecretory insulin-producing cells (IPCs) from the brains of wandering third instar larvae. Immunoreactivity for dILP2 produced in IPCs is expected to be lower when more of it is released into the hemolymph. We found that the average intensity of dILP2 immunostaining in the IPCs was not lower in *dPIP4K*^{29} compared to controls; instead, it showed a small but significant increase (Fig. 2E(i) and (ii)). Thus, we found no evidence of elevated production or release of dILPs in 3rd instar larvae that might explain the increased PIP_3 levels observed in *dPIP4K*^{29}. Further, we observed that *InR* receptor mRNA levels were also not different between *dPIP4K*^{29} and wildtype indicating that levels of InR that are activated by dILPs are also not likely to be different between the two genotypes (Fig. 2D). Collectively, our experiments show plasma membrane PIP_3 levels to be elevated in cells lacking dPIP4K without an increase in dILP secretion or cellular insulin receptor levels.

dPIP4K^{29} cells are intrinsically more sensitive to insulin stimulation.

We developed *ex-vivo* assays to test the sensitivity of tissues dissected from 3rd instar larvae to stimulation with bovine insulin. It has previously been shown that *Drosophila* cells stimulated with bovine insulin respond using signal transduction elements conserved with those proposed for the canonical mammalian insulin signalling pathway (Lizcano et al., 2003). We observed that in salivary glands and fat body dissected from 3rd instar larvae, *ex-vivo* insulin stimulation triggered a rise in plasma membrane PIP_3 levels, measured using the GFP::PH-GRP1 probe. Following insulin stimulation (10 min, 10 μM), the rise in PIP_3 levels in *dPIP4K*^{29} was higher than in wild type (Fig. 3A(i), A(ii)). This increased PIP_3 production was also seen in salivary gland cells (Fig. 3C(ii)) where the dPIP4K protein had been selectively depleted using salivary gland specific RNAi (Fig. 3C(i)). The increased sensitivity of *dPIP4K*^{29} cells to *ex-vivo* insulin stimulation could be reverted by specifically reconstituting dPIP4K in salivary gland cells (Fig. 3D). Overexpression of dPIP4K in wild-type salivary gland cells resulted in reduced levels of insulin stimulated PIP_3 levels (Fig. 3E). A similar observation was made in fat body cells where

211 PIP_3 production increased with stimulation over a wide range of insulin concentrations used. Fat body
212 lobes dissected from starved larvae were stimulated with over a 100-fold range of insulin concentrations.
213 While 100 nM of insulin barely elicited an increase in plasma membrane PIP_3 levels, we observed that
214 *dPIP4K*^{29} fat cells show a larger rise in PIP_3 levels compared to the controls at higher concentrations(Fig.
215 3C(i)-(iii)).
216
217 **Quantitative measurements of PIP_3 mass in *Drosophila* larvae**
218 To test if the probe-based imaging of PIP_3 in single cells indeed reflects *in vivo* changes across the animal,
219 we refined and adapted existing protocols (Clark et al., 2011) to perform mass spectrometric
220 measurements of PIP_3 from *Drosophila* whole larval lipid extracts. The amount of PIP_3 that has been
221 detected and quantified from biological samples is in the range of a few tens of picomoles (Malek et al.,
222 2017). We coupled liquid chromatography to high sensitivity mass spectrometry (LCMS) and used a
223 Multiple Reaction Monitoring (MRM) method to detect PIP_3 standards for reliable quantification down
224 to a few femtomoles (ca. 10 fmol, the lowest point in the figure inset on the standard curve in Fig. 3,
225 Supplement 1, (A). Since cellular lipids are composed of molecular species with varying acyl chain
226 lengths, we first characterized the PIP_3 species from *Drosophila* whole larval extracts through use of
227 neutral loss scans and thereafter quantified the abundance of these species. Fig. 3, Supplement 1, (B)
228 depicts the elution profiles of the different PIP_3 species that were reproducibly detected across samples
229 and Fig. 3, supplement 2, (A) shows the relative abundance of various PIP_3 species. The 34:2 PIP_3 species
230 was found to be the most abundant. In a pilot experiment, we bisected whole larvae, stimulated them
231 with insulin and measured the levels of various PIP_3 species between samples with and without insulin
232 stimulation. Our LCMS method could clearly detect an increase in the levels of several PIP_3 species upon
233 insulin stimulation (Fig. 3, supplement 2, (B)).
234
235 Using this method, we compared PIP_3 levels from whole larval lipid extracts of various genotypes
236 following insulin stimulation. We observed that compared to controls, *dPIP4K*^{29} larvae showed higher
237 PIP_3 levels upon insulin stimulation (Fig. 3F(i), F(ii)). Similarly, upon pan-larval knockdown of dPIP4K
238 by RNAi (Fig. 3, supplement 2, C(i)) enhanced PIP_3 levels were observed following insulin stimulation
239 (Fig. 3, supplement 2, C(ii) and (iii)) although the differences were not as striking as seen in *dPIP4K*^{29};
240 presumably this reflects the residual and variable amounts of dPIP4K protein seen during RNAi based
241 knockdown (Fig. 3, supplement 2, C(i)). We also performed pan-larval rescue of dPIP4K protein in

242 *dPIP4K*^{29} larvae and observed a rescue in levels of various PIP_3 species (Fig. 3, supplement 2, D(i) and
243 D(ii)). Finally, we also depleted dPIP4K in *Drosophila* S2 cells (Fig. 3G(ii)) in culture using two
244 independent dsRNA treatments and found that on insulin stimulation of serum starved cells, the total
245 level of PIP_3 was enhanced compared to that in control cells (Fig. 3G(i)); the levels of individuals species
246 of PIP_3 underlying this elevation broadly reflected those seen in experiments with Drosophila larval
247 extracts (Fig. 3G (iii)). Together, the observations from these two independent assays (fluorescent probe
248 based PIP_3 measurement and mass spectrometry) suggests that in dPIP4K depleted cells, increased
249 amounts of PIP_3 are produced at the plasma membrane during insulin stimulation, thus implying that
250 *dPIP4K* negatively regulates PIP_3 production in this setting.
251
252 **dPIP4K supports TORC1-mediated feedback inhibition on insulin receptor signalling**
253 We had previously reported a systemic reduction in TORC1 activity in *dPIP4K*^{29} larvae. It is well
254 understood in mammalian cells that TORC1 activation can mediate feedback inhibition on insulin
255 receptor substrate (IRS) through phosphorylation to suppress insulin signalling. In *Drosophila*, such
256 feedback inhibition has been partly demonstrated (Kockel et al., 2010), though its precise mechanism is
257 unclear. To understand if there was a relationship between reduced TORC1 output (Gupta et.al, 2013)
258 and the increased insulin-stimulated PIP_3 production in *dPIP4K*^{29} cells (*this study*), we studied the effect
259 of tissue-specific manipulation of TORC1 activity on insulin-stimulated PIP_3 production in salivary
260 gland cells. For this, we down-regulated Rheb, the GTPase that directly binds and activates TORC1 (Tee
261 et al., 2003). In *AB1>Rheb*^{RNAi} glands, cell size is substantially reduced consistent with the known
262 requirement for TORC1 signalling in regulating cell size (Fig. 4A (i)). Following insulin stimulation of
263 *AB1>Rheb*^{RNAi} glands, PIP_3 levels at the plasma membrane were elevated compared to controls (Fig. 4A
264 ii). Conversely, we compared PIP_3 production in control cells and those selectively overexpressing Rheb
265 (*AB1>dRheb*) that is expected to enhance TORC1 signalling activity. Following insulin stimulation, the
266 levels of PIP_3 generated were significantly lower in *AB1>dRheb* glands compared to controls (Fig. 4B (i),
267 (ii)). Similarly, knockdown of TSC, the GTPase activating protein (GAP) for Rheb, expected to result in
268 hyperactivation of Rheb (Zhang et al., 2003), also reduces the PIP_3 levels seen post insulin stimulation
269 (Fig. 4C (i), (ii)). Thus, TORC1 output can control plasma membrane PIP_3 levels during insulin
270 signaling in salivary gland cells.
271

We also tested the requirement for dPIP4K in TORC1-mediated control of PIP_3 levels during insulin stimulation. When dPIP4K function is reconstituted in salivary glands (*AB1>dPIP4K; dPIP4K^{29}*), as expected, normal levels of insulin-stimulated PIP_3 production were restored (refer Fig. 3D). Knockdown of *dRheb* in salivary glands resulted in a further elevation of insulin-stimulated PIP_3 levels over that seen in *dPIP4K^{29}* (Fig. 4D(i), (ii)). However, when *dRheb* was overexpressed in *dPIP4K^{29}* salivary glands; (*AB1>dRheb; dPIP4K^{29}*), surprisingly, we found that insulin-stimulated PIP_3 levels were not lower than in *AB1>; dPIP4K^{29}* (Fig. 4E (i), (ii)). Likewise, depletion of TSC in *dPIP4K^{29}* (*AB1>Tsc^{RNAi}; dPIP4K^{29}*) did not lower insulin stimulated PIP_3 levels (Fig. 4F (i), (ii)). Thus, dPIP4K function facilitates TORC1-mediated feedback inhibition of PIP_3 levels during insulin stimulation. Upon loss of dPIP4K, the inhibitory action of TORC1-mediated feedback upon insulin signalling is insufficient to generate normal levels of PIP_3.

PIP4K is required at the plasma membrane to control of insulin-stimulated PIP_3 production

We and others have previously shown that PIP4Ks localize to multiple subcellular membrane compartments (Clarke et al., 2010; Gupta et al., 2013). It is also reported that the substrate for this enzyme i.e. PI5P is present on various organellar membranes inside cells (Sarkes and Rameh, 2010). To further probe the mechanism of regulation of PIP_3 levels by dPIP4K, we decided to identify the sub-cellular compartment at which dPIP4K function is required to regulate PIP_3 levels. We generated transgenic flies to target dPIP4K to specific subcellular compartments (Fig. 5A). Using unique signal sequences, we targeted dPIP4K specifically to the plasma membrane (Fig. 5B (ii)), endomembrane compartments viz. the ER and Golgi (Fig. 5B (iii)) and the lysosomes (Fig. 5B (iv)). Lysates from S2R+ cells expressing these constructs for assayed for PIP4K activity and we found that all of the targeted dPIP4K enzymes were active (Fig. 5C(i), C(ii)); activity was proportional to the amount of protein expressed. Each of these targeted dPIP4K constructs were selectively reconstituted into dPIP4K null (*dPIP4K^{29}*) cells and tested for its ability to revert the enhanced insulin-stimulated PIP_3 production of *dPIP4K^{29}*. For this, we stimulated dissected salivary glands *ex-vivo* with insulin and measured PIP_3 production using the GFP::PH-GRP1 probe. Under these conditions, while endomembrane (Fig. 5E) and lysosome-targeted (Fig. 5F) dPIP4K failed to revert the elevated PIP_3 levels of *dPIP4K^{29}*, reconstitution with the plasma-membrane targeted dPIP4K completely restored the elevated PIP_3 levels in *dPIP4K^{29}* to that of controls (Fig. 5D). Further, overexpression of plasma-membrane targeted dPIP4K in wildtype salivary gland cells resulted in lower insulin stimulated PIP_3 levels compared to the controls

303 at 5 mins post insulin stimulation (Fig. 5G). These observations suggest that plasma membrane localized
304 dPIP4K is sufficient to regulate insulin-stimulated PIP_3 production.
305
306 We also tested the ability of plasma membrane localized PIP4K to regulate PIP3 production during
307 insulin signalling. In a previous study, overexpression of human PIP4K2B in CHO-IR cells was shown
308 to reduce the levels of $pAKT^{T308}$, an important PIP_3 dependent signalling event during insulin
309 stimulation (Carricaburu et al., 2003). We tested the effect of overexpressing plasma membrane
310 restricted PIP4K2B in these cells on $pAKT^{T308}$ during insulin stimulation. We generated a PIP4K2B
311 construct with a CAAX-motif at its C-terminus (PIP4K2B::$mCherry^{CAAX}$) that localized the enzyme to
312 the plasma membrane as expected, while the wildtype PIP4K2B (PIP4K2B::eGFP) can be seen at various
313 subcellular compartments (Fig. 5H(i)). CHO-IR cells transiently overexpressing either PIP4K2B::eGFP
314 or PIP4K2B::$mCherry^{CAAX}$ were serum starved, stimulated with insulin and $pAKT^{T308}$ was measured
315 through immunoblotting. As previously reported, we found that PIP4K2B::eGFP overexpression
316 resulted in a small but significant decrease in $pAKT^{T308}$ (Fig. 5H'). Interestingly, consistent with our
317 findings in *Drosophila* larval cells, we observed that over-expressed PIP4K2B::$mCherry^{CAAX}$ also caused
318 a decrease in $pAKT^{T308}$. In fact, this decrease was achieved despite lower levels of expression of
319 PIP4K2B::$mCherry^{CAAX}$ compared to the wildtype protein. Thus, PIP4K2B activity at the plasma
320 membrane is sufficient to negatively regulate PIP_3 dependent $pAKT^{T308}$ levels in mammalian cells.
321
322 **dPIP4K alters PIP_3 turnover by modifying Class I PI3K activity**
323 PIP_3 levels at the plasma membrane upon insulin stimulation also depend on the length of time the
324 receptor remains activated. Our 10-min stimulation protocol was based on earlier studies performed on
325 *Drosophila* S2 cell-cultures where the response to insulin was maximal at 10 min (Lizcano et al., 2003).
326 However, in order to check for any differences in the dynamics of response to insulin, we also studied
327 the time course of PIP_3 elevation following increasing times of insulin stimulation *ex-vivo*. Comparison
328 of fixed preparations of salivary glands expressing GFP-PH-GRP1 probe showed a comparable time
329 course of PIP_3 elevation but higher PIP_3 levels at every time point in $dPIP4K^{29}$ than in control glands
330 (Fig. 6, Supplement 1, (i) and (ii)). To understand the effect of dPIP4K on insulin signaling at the plasma
331 membrane with increased temporal resolution, we developed a live-imaging assay to follow the
332 dynamics of PIP_3 turnover using the PH-GRP1 probe in salivary gland cells. A schematic of the reactions
333 involved in the process and the assay protocol is depicted in Fig. 6A(i) and (ii). In this assay, during

insulin stimulation, the dynamics of PIP_3 turnover has three phases – (i) Rise phase – PIP_3 levels increase after a stimulus owing to the activation of PI3K and relatively lower phosphatase activity (ii) Steady-state phase – the opposing kinase and phosphatase activities regulating PIP_3 levels balance out each other (iii) Decay phase - PI3K activity is irreversibly inhibited by wortmannin while PIP_3 phosphatases remain active. A single experimental trace is shown in Fig. 6B (i); insulin stimulation triggers a rise in PIP_3 levels that peak and subsequently decline. Addition of wortmannin prior to addition of insulin abolished insulin stimulated PIP_3 production establishing the effectiveness of Class I PI3K inhibition in this assay (Fig. 6B(ii)).

We tested the effect of loss of dPIP4K and tissue-specific overexpression of dPIP4K on PIP_3 turnover. Loss of dPIP4K resulted in higher steady state levels of PIP_3 in salivary gland cells compared to controls (Fig. 6C) while overexpression of dPIP4K resulted in lower steady-state levels of PIP_3 (Fig. 6D). These findings are consistent with the results from our imaging of PIP_3 levels from fixed salivary glands of these genotypes (see Fig 3 A(ii) and E). We also analyzed the rate of change in PIP_3 levels during the initial phase following insulin stimulation. This analysis clearly revealed an enhanced rate of PIP_3 production on loss of *dPIP4K*^{29} relative to controls and a reduced rate of PIP_3 production in cells overexpressing this enzyme (Fig. 6E(i)). Thus, dPIP4K has the ability to modulate the rate of PIP_3 production during insulin stimulation. A similar analysis of the rate of decrease in PIP_3 levels during the phase after wortmannin addition (i.e when Class I PI3K activity has been inhibited) showed a marginally slower rate of decay in PIP_3 levels in both dPIP4K depleted cells relative to controls but also in cells overexpressing dPIP4K (Fig. 6E(ii)). This finding implies that dPIP4K function is also able to modulate the PIP_3 phosphatase activity operative during insulin signalling in *Drosophila* salivary gland cells although less substantially than its effect on Class I PI3K activity.

dPIP4K function regulates sugar metabolism during larval development.

We tested if increased sensitivity to insulin seen in *dPIP4K*^{29} had any impact on the physiological response of the animals to sugar intake. It has previously been reported that larvae raised on a high sugar diet (HSD) develop an insulin resistance phenotypes reminiscent of Type II diabetes (Musselman et al., 2011; Pasco and Léopold, 2012). At the level of the organism, this includes reduced body weight, a developmental delay and elevated levels of hemolymph trehalose, the main circulating sugar in insect hemolymph. As previously reported, we found that when grown on HSD (1M sucrose), wild-type larvae

show ca. 9 days delay in development compared to animals grown on normal food (0.1M Sucrose) (Fig. 7A). However, interestingly, in *dPIP4K*^{29} larvae grown on HSD a delay of only 5 days was seen compared to the same genotype grown on 0.1M sucrose (Fig. 7A). We also biochemically measured the levels of circulating trehalose in the hemolymph of wandering third instar larvae. It was observed that *dPIP4K*^{29} larvae raised on normal food, showed circulating trehalose levels are *ca.* 40% lower compared to controls. Further, when wild-type animals were grown on HSD, circulating trehalose levels in larvae were elevated by ca. 25 % compared to that on normal food (Fig. 7B). However, when *dPIP4K*^{29} larvae were raised on HSD, circulating trehalose levels remained essentially unchanged (Fig. 7B) compared to that in animals grown on normal food. Together, these observations suggest that loss of dPIP4K in larvae confers partial protection against phenotypes that arise when challenged with a high sugar diet.

Discussion

The generation of PIP_3 is a conserved element of signal transduction by many growth factor receptors. The enzymes that control PIP_3 levels during this process, namely Class I PI3K and the lipid phosphatases PTEN and SHIP2 are well studied and the biological consequences of mutations in genes encoding these enzymes underscore the importance of tight regulation of PIP_3 levels during growth factor signalling. While the roles of many of the core enzymes that are directly involved in PIP_3 metabolism have been studied extensively, the function of proteins that regulate their activity remains less understood; to date regulation of Class I PI3K activity by small GTPases (Ras, Rac) and $G_{\beta\gamma}$ subunits has been described [reviewed in (Hawkins and Stephens, 2015)]. Although a role for PIP4K enzymes in regulating growth factor signalling through PIP_3 generation has been reported by several studies (Bulley et al., 2016; Carricaburu et al., 2003; Lamia et al., 2004), the biochemical mechanism and cell-biological context in which they do so has remained obscure. PIP4Ks convert PI5P to $PI(4,5)P_2$ but to date no study has found a role for PIP4K in regulating overall cellular $PI(4,5)P_2$ levels [reviewed in (Kolay et al., 2016)]. One possibility that has been raised is that PIP4Ks may generate the $PI(4,5)P_2$ pool from which PIP_3 is produced by Class I PI3K activity. Although PI5P, the preferred substrate of PIP4K, is a low abundance lipid, in principle, it is possible that a small, local pool of $PI(4,5)P_2$ is generated from PI5P by PIP4K an d the loss of this small pool of $PI(4,5)P_2$ is not detected by the mass assays for estimating total cellular levels of this lipid. Quantitatively, based on their relative abundance, the small PIP4K generated pool of $PI(4,5)P_2$ is likely to be sufficient to serve as the substrate for PIP_3 generation by Class I PI3K. A recent study (Bulley et al., 2016) has reported that PIP_3 levels are reduced in immortalized B-cells in which

PIP4K2A activity is down regulated. By contrast, it has been previously reported that loss of PIP4K2B in mice results in increased levels of insulin signalling readouts such as $pAKT^{308}$ that are direct correlates of PIP_3 levels (Lamia et al., 2004). The exact reasons for these conflicting results is unclear and may include the different cell types used in each study; a key reason is likely to be the overlapping function of the three PIP4K isoforms present in mammalian genomes. In this study, we found that in *Drosophila*, that contains only a single gene encoding PIP4K activity (dPIP4K)(Balakrishnan et al., 2015; Gupta et al., 2013), the levels of plasma membrane PIP_3 in cells lacking dPIP4K were elevated compared to controls. We established this finding using both a fluorescent reporter for plasma membrane PIP_3 in single cell assays using multiple cell types and also using lipid mass spectrometry across larval tissues and cultured, dPIP4K depleted *Drosophila* S2 cells. Thus, our study clearly demonstrates that in *Drosophila*, dPIP4K function is a negative regulator of PIP_3 production during growth factor stimulation. The elevated PIP_3 levels seen when dPIP4K is depleted are not consistent with a role for this enzyme in generating the $PI(4,5)P_2$ at the plasma membrane used by Class I PI3K as substrate to generate PIP_3 during insulin signalling. Therefore, is likely that dPIP4K regulates PIP_3 levels through its ability to control the function of proteins that themselves regulate PIP_3 levels during Class I PI3K signalling.

In an earlier study (Gupta et al., 2013), we had observed *dPIP4K*^{29} larvae to have systemically reduced levels of TOR activation. In mammalian cells, reducing TOR activity through the use of rapamycin or a loss of S6K, a direct target of TORC1, leads to increased activation of insulin signalling pathway and obesity resistance which was associated with increased insulin sensitivity (Haruta et al., 2000; Reilly et al., 2011; Um et al., 2004). It is also reported that S6K inactivates IRS-1 by phosphorylating it on multiple serine residues (Gual et al., 2005; Tremblay et al., 2007). Therefore, it is reasonable to hypothesize a scenario where the reduced TORC1 activity in *dPIP4K*^{29} cells may be the defect that drives the increase in the levels of PIP_3 in *dPIP4K*^{29}. An alternative explanation of our observations is that loss of dPIP4K could uncouple the negative feedback from TORC1 activity to PIP_3 generation at the plasma membrane. In this study, we found that in wild-type larval cells, modulating TORC1 activity could tune PIP_3 levels during insulin stimulation (Fig 4 A-C); enhancing TORC1 output resulted in lower levels of insulin-induced PIP_3 whereas reducing TORC1 activity caused higher levels of PIP_3. By contrast, overexpression of Rheb or the down-regulation of Tsc1/2 was not able to revert the elevated plasma membrane PIP_3 levels in *dPIP4K*^{29} cells (Fig 4 E-F) although they were able to restore the reduced cell size in *dPIP4K*^{29}

(Fig. 4, Supplement 1, (A) and (B)). These results imply two conclusions: 1) Decreased TORC1 activity is not sufficient to explain the enhanced PIP_3 levels in *dPIP4K*^{29} larval cells and 2) Efficient feedback regulation of PIP_3 levels by TORC1 outputs following Rheb activation requires intact dPIP4K function.

Binding of insulin to its receptor triggers a signalling cascade where the initial events occur at the plasma membrane. These involve interaction of the activated insulin receptor-ligand complex with IRS followed by the recruitment and activation of Class I PI3K at the plasma membrane. At which sub-cellular location is dPIP4K activity required to regulate this process? Fractionation and immunolocalization studies in mammalian cells (Clarke et al., 2010) and *Drosophila* (Gupta et al., 2013) have indicated that PIP4K isoforms are distributed across multiple subcellular compartments including the plasma membrane, nucleus and internal vesicular compartments. In this study, using selective reconstitution of the dPIP4K to specific membrane compartments, in cells devoid of any endogenous PIP4K protein, we found that plasma membrane targeted dPIP4K could rescue the elevated PIP_3 levels in dPIP4K null cells. This observation strongly suggests that the plasma membrane localized dPIP4K is sufficient to control PIP_3 production during insulin stimulation. Our observation that *dPIP4K*^{29} cells were hypersensitive to overexpression of *dINR* or *chico* compared to wild-type cells likely reflects the loss of a dPIP4K dependent event in the control of PIP_3 levels at the plasma membrane. Overexpression of plasma-membrane localized PIP4K2B was able to reduce $pAKT^{308}$ phosphorylation upon insulin stimulation in mammalian cells just as well as the wildtype PIP4K2B enzyme. Our finding of a role for the plasma membrane localized PIP4K in regulating PIP_3 levels in both *Drosophila* and mammalian cells underscores the evolutionarily conserved nature of this mechanism. Previous studies have shown that levels of PI5P, the substrate for PIP4Ks, increases upon insulin stimulation and importantly, addition of exogenous PI5P can stimulate glucose uptake in a PI3K-dependent manner (Grainger et al., 2011; Jones et al., 2013). Therefore, plasma membrane localized PIP4K and the levels of its substrate PI5P could be a mechanism by which early events during insulin signalling are regulated.

What molecular event involved in PIP_3 turnover might dPIP4K regulate at the plasma membrane? Using live cell imaging studies of PIP_3 turnover at the plasma membrane coupled with chemical inhibition of Class I PI3K, we were able to observe that dPIP4K function has a substantial impact on the rate of PIP_3 production following insulin stimulation whereas the rate of PIP_3 degradation was only marginally affected. This finding suggests that dPIP4K likely regulates the activity of Class I PI3K either directly or

by controlling its coupling to the activated insulin receptor complex at the plasma membrane; the mechanism by which it does so remains to be established.

What might be the physiological consequence of losing dPIP4K mediated feedback control on PIP_3 production in the context of insulin signalling? Previous studies in mouse and human cells have reported that excessive activation of TORC1 signalling leads to inactivation of insulin signalling pathway and development of insulin resistance (Harrington et al., 2004; Shah et al., 2004; Tzatsos and Kandror, 2006). Since TORC1 activity is reduced (Gupta et al., 2013) and PIP_3 were elevated (this study) in animals lacking dPIP4K, it is likely that loss of dPIP4K impacts sugar metabolism in *Drosophila* larvae. Using a recently reported high-sugar induced obesity and Type II diabetes-like disease model in *Drosophila* (Musselman et al., 2011), we found that *dPIP4K*^{29} larvae appear resistant to a high sugar diet as measured by the elevation in the hemolymph trehalose levels and they were relatively resistant to the developmental delay seen when wild-type larvae are reared on a high-sugar diet. This observation is reminiscent of that reported for the PIP4K2B$^{-/-}$ mice that have a reduced adult body weight compared to controls and clear blood glucose faster following a sugar bolus than control animals (Lamia et al., 2004). Our observation that dPIP4K at the plasma-membrane controls sensitivity to insulin receptor activation suggests a molecular basis for the physiological phenotypes observed in *dPIP4K*^{29} larvae and PIP4K2B$^{-/-}$ mice. These observations also raise the possibility that inhibition of PIP4K activity may offer a route to reducing insulin resistance in the context of Type II diabetes. Such a mechanism may explain the hyperactivation of the T-cell receptor responses in mice lacking PIP4K2C (Shim et al., 2016), since the activation of Class I PI3K is a key element of T-cell receptor signal transduction. More generally, PIP4K activity likely offers a novel element of regulation for Class I PI3K activity in the context of receptor tyrosine kinase signalling.

Materials and Methods

Drosophila strains and rearing –

Unless indicated, flies were grown on standard fly medium containing corn meal, yeast extract, sucrose, glucose, agar and antifungal agents. For all experiments, crosses were setup at 25°C in vials/bottles under non-crowded conditions.

Fly medium composition:

Ingredients	0.1 M sucrose	1 M sucrose
For 1 Litre		
Corn flour	80 g	80 g
D-Glucose	20 g	20 g
Sugar	40 g	342 g
Agar	8 g(4g)	8 g
Yeast powder	15 g	15 g
Propionic acid	4 ml	4 ml
TEGO(Methyl parahydroxy benzoate)	0.7 g	0.7 g
Orthophosphoric acid	0.6 ml	0.6 ml

The following stocks were used in the study: wildtype strain Red Oregon R (ROR), AB1-Gal4 (Bloomington # 1824), *UAS-dInR* (Bloomington # 8262), *UAS-Rheb*^{RNAi} (Bloomington TRiP # 33966), *UAS-Rheb* (Bloomington # 9688), *UAS-TSC*$^{RNA\ i}$(Bloomington TRiP # 52931), P{tGPH}4 (Bloomington # 8164), UAS-*dPIP4K*^{RNAi} (Bloomington TRiP # 65891). *UAS-dPIP4K::eGFP* and *dPIP4K*^{29} were generated in the lab and described in (Gupta et al., 2013). For PIP_3 measurements in the *dPIP4K*^{29} rescue experiment (Fig. 4F) using GFP-PH-GRP1 probe, we cloned dPIP4K cDNA (BDGP clone# LD10864) into pUAST-attB between *EcoRI* and *XhoI* sites without the GFP tag. The generation of flies expressing dPIP4K::-mCherry-CAAX is described in *Kumari K et.al, 2017*. For targeting dPIP4K to the endomembranes, the sequence QGSMGLPCVVM (*Sato.M et. al., 2006*) replaced the CAAX motif in the dPIP4K::mCherry-CAAX construct. To generate Lysosomal-dPIP4K::eGFP, the 39 amino-acid sequence from p18/LAMTOR (*Menon S et.al., 2014*) was used as a signal sequence. The signal sequence was commercially synthesized with a C-terminal flag tag and introduced upstream of dPIP4K::eGFP.

505 The entire fusion construct was cloned into pUAST-attB by GIBSON assembly using *NotI* and *XbaI*
506 sites. All transgenic lines were generated using insertions that were performed using site-specific
507 recombination. The level of GFP fluorescence from lysosomal-dPIP4K::eGFP was observed to be very
508 low in the salivary glands and did not interfere with our analysis PIP_3 measurements using the GFP-PH-
509 GRP1 probe in Fig. 6F.
510
511 **Cell Culture, dsRNA treatment and Insulin stimulation assays –**
512 CHO cell line stably expressing insulin receptor (isoform A) was a kind gift from Dr Nicholas Webster,
513 UCSD. These were maintained at standard conditions in HF12 culture medium supplemented with 10%
514 Fetal bovine serum and under G418 selection (400 µg/ml). Transfections were done 48 hrs. before the
515 assay using FuGene, Promega Inc. as per manufacturer's protocols when the cultures were 50%
516 confluent. For insulin stimulation assays, cells were starved overnight in HF12 medium without serum.
517 Thereafter, the cells were de-adhered, collected into eppendorf tubes and stimulated with 1 µM insulin
518 for indicated times. Post stimulation, cells were spun down and immediately lysed. For dsRNA
519 treatments, 0.5 X 10^6 cells were seeded into a 24-well plate. Once observed to be settled, cells were
520 incubated with incomplete medium containing 1.875 µg of dsRNA. After 1 hour, an equal amount of
521 complete medium was added to each well. The same procedure was repeated on each well 48 hours after
522 initial transfection after removal of the spent medium from each well. Cells were harvested by
523 trypsinization after a total of 96 hours of dsRNA treatment. For mass spectrometric estimation of PIP_3,
524 S2R+ cells were pelleted down and stimulated with 1 µM insulin for 10 min. The reaction was stopped
525 by the addition of ice-cold initial organic mix (described later in the section) and used for lipid
526 extraction.
527
528 **Larval growth Curve Analysis** -
529 Adult flies were made to lay eggs within a span of 4-6 hrs on normal food. After 24 hrs, newly hatched
530 first instar larvae were collected and transferred in batches of about 15-25 larvae per into vials containing
531 either 0.1/1M Sucrose in the fly media with other components unaltered. The vials were then observed
532 to count the number of pupae.
533
534
535

Hemolymph Trehalose Measurements –

The measurements were done exactly as described in (Musselman et al., 2011). In brief, hemolymph was pooled from five to eight larvae to obtain 1 µl for assay. The reagents used porcine trehalase (SIGMA, T8778) and GO kit (SIGMA, GAGO20)

Cell size analysis in salivary glands -

Salivary glands were dissected from wandering third instar larvae and fixed in 4% paraformaldehyde for 30 min at 4°C. Post fixation, glands were washed thrice with 1X PBS and incubated in BODIPY-FL-488 for 3 hours at room temperature. The glands were washed thrice in 1X PBS following which nuclei were labelled (using either DAPI or TOTO3) for 10 mins at room temperature and washed with 1X PBS again. The glands were then mounted in 70% glycerol and imaged within a day of mounting. Imaging was done on Olympus FV1000 Confocal LSM using a 20x objective. The images were then stitched into a 3D projection using an ImageJ plugin. These reconstituted 3D z-stacks were then analyzed for nuclei numbers (correlate for cell number) and volume of the whole gland using Volocity Software (version 5.5.1, Perkin Elmer Inc.). The average cell size was calculated as the ratio of the average volume of the gland to the number of nuclei.

***Ex vivo* insulin stimulation and PIP_3 measurements in salivary glands and fat body** -

For experiments with salivary glands, wandering third instar larvae were dissected one larva at a time and glands were immediately dropped into a well of a 96-well plate containing either only PBS or PBS + 10 µM Insulin (75 µl) and incubated for 10 min at RT. Following this, 25 µl of 16% PFA was added into the same well to yield a final conc. of 4% PFA. The glands were fixed in this solution for 18 min at room temperature and then transferred sequentially to wells containing PBS every 10 min for 3 washes. Finally, glands were mounted in 80% glycerol in PBS containing antifade (0.4% propyl-gallate). For experiments with fat body lobes, late third instar feeding larvae were starved by placing them on a filter paper soaked in 1X PBS for 2 hrs. Thereafter, the incubation, fixation and mounting steps were done exactly as described for salivary glands. Imaging was done on LSM 780 inverted confocal microscope with a 20X/0.8 NA Plan Apochromat objective. For quantification, confocal slices were manually curated to generate maximum z-projections of middle few planes of cells. Thereafter, line profiles were drawn across clearly identifiable plasma membrane regions and their adjacent cytosolic regions and ratios of mean intensities for these line profiles were calculated for each cell. For salivary glands, about 10-15 cells

567 from multiple glands were analyzed and used to generate statistics. For fat body, about 50 cells each from
568 multiple animals were used for analysis.
569
570 For live imaging, salivary glands from wandering third instar larvae were dissected (glands from one
571 larva imaged in one imaging run) and placed inside a drop of imaging buffer (1X PBS containing 2mg/ml
572 glucose) on a coverglass. The buffer was carefully and slowly soaked out with a paper tissue to let the
573 glands settle and adhere to the surface. Thereafter, the glands were immediately rehydrated with 25 µl
574 of imaging buffer. The imaging was done on Olympus FV3000 LSM confocal system using a 10X
575 objective. A total of 80 frames of a single plane were acquired, with 10s intervals. While imaging, 25 µl
576 of 20uM (2X) bovine insulin was used to stimulate the glands. After the steady state was achieved, 50 µl
577 of 800nM (2X) of wortmannin was added on top to inhibit PI3K activity.
578
579 **PIP_3 measurement by LC-MS/MS –**
580 The method was adopted and modified as required from (Clark et al., 2011).
581 **Lipid extraction –**
582 5 larvae were dissected in 1X PBS and transferred immediately into 37.5 µl of 1X PBS in a 2 ml
583 Eppendorf. For insulin stimulation, to this, 37.5 µl of 100 µM Insulin (final concentration – 50 µM) was
584 added and the tube was incubated on a mix mate shaker for 10 min at 500 rpm. At the end of incubation
585 time, 750 µl of ice-cold 2:1 MeOH:$CHCl_3$ organic mix was added to stop the reaction. Part of this
586 solution was decanted and the rest of the mix containing larval tissues was transferred into a
587 homogenization tube. Larval tissues were homogenized in 4 cycles of 10 secs with 30 sec intervals at
588 6000 rpm in a homogenizer (Precellys, Bertin Technologies). The tubes were kept on ice at all intervals.
589 The entire homogenate was then transferred to a fresh eppendorf and the homogenization tube was then
590 washed with the decanted mix kept aside earlier. 120 µl of water was added to the homogenate collected
591 in eppendorf, followed by addition of 5 ng of 17:0, 20:4 PIP_3 internal standard (ISD). The mixture was
592 vortexed and 725 µl of chloroform was added to it. After vortexing again for 2 min at around 1000-1500
593 rpm, the phases were separated by centrifugation for 3 min at 1500g. 1ml of lower organic phase was
594 removed and stored in a fresh tube. To the remaining aqueous upper phase, again 725 µl of chloroform
595 was added. The mixture was vortexed and spun down to separate the phases. Again, 1 ml of the organic
596 phase was collected and pooled with the previous collection (total of 2ml). This organic phase was used
597 for measuring total organic phosphate. To the aqueous phase, 500 µl of the initial organic mix was added

598 followed by 170 µl of 2.4M HCl and 500 µl of $CHCl_3$. This mixture was vortexed for 5 min at 1000-1500
599 rpm and allowed to stand at room temperature for 5 minutes. The phases were separated by
600 centrifugation (1500g, 3 min). The lower organic phase was collected into a fresh tube by piercing
601 through the protein band sitting at the interface. To this, 708 µl of lower phase wash solution was added,
602 the mixture was vortexed and spun down (1500g, 3 min). The resultant lower organic phase was
603 completely taken out carefully into an Eppendorf tube and used for derivatization reaction.
604
605 **Extraction solvent mixtures:**
606 Initial organic mix: MeOH/Chloroform in the ratio of 484/242 ml, Lower Phase Wash Solution:
607 Methanol/1 M hydrochloric acid/ chloroform in a ratio of 235/245/15 ml. All ratios are expressed as
608 vol/vol/vol.
609
610 **Derivatization of Lipids –**
611 To the organic phase of the sample, 50 µl of 2M TMS-Diazomethane was added (TO BE USED WITH
612 ALL SAFETY PRECAUTIONS!). The reaction was allowed to proceed at room temperature for 10 min
613 at 600 rpm. After 10 min, 10 µl of Glacial acetic acid was added to quench the reaction, vortexed briefly
614 and spun down. 700 µl of post derivatization wash solvent was then added to the sample, vortexed (2
615 min, 1000-1500 rpm) and spun down. The upper aqueous phase was discarded and the wash step was
616 repeated. To the final organic phase, 100 µl of 9:1 MeOH:H_2O mix was added and the sample was dried
617 down to about 10-15 µl in a speedvac under vacuum.
618
619 **Chromatographic separation and Mass spectrometric detection –**
620 The larval lipid extracts were re-suspended in 170 µl LC-MS grade methanol and 30 µl LC-MS grade
621 water. Samples were injected as duplicate runs of 3.5 µl. Chromatographic separation was performed on
622 an Acquity UPLC BEH300 C4 column (100 x 1.0 mm; 1.7 µm particle size) purchased from Waters
623 Corporation, USA on a Waters Aquity UPLC system and detected using an ABSCIEX 6500 QTRAP
624 mass spectrometer. The flow rate was 100 µL/min. Gradients were run starting from 55% Buffer A
625 (Water + 0.1% Formic Acid)- 45% Buffer B (Acetonitrile + 0.1% Formic acid) to 42% B from 0-5 min;
626 thereafter 45% B to 100% B from 5-10 min; 100% B was held from 10-15 min; brought down from 100%
627 B to 45% B between 15-16 min and held there till 20th min to re-equilibrate the column. On the mass
628 spectrometer, in pilot standardization experiments, we first employed Neutral Loss Scans on biological

samples to look for parent ions that would lose neutral fragments of 598 a.m.u indicative of PIP_3 lipid species (as described in (Clark et al., 2011)). Thereafter, these PIP_3 species were quantified in biological samples using the selective Multiple Reaction Monitoring (MRM) method in the positive mode. Only those MRM transitions that showed an increase upon insulin stimulation of biological samples were used for the final experiments (depicted in figure S3B). The MRM transitions for the different PIP_3 species quantified are listed out in the table below. Area of all the peaks was calculated on Sciex MultiQuant software. The area of the internal standard peak was used to normalize for lipid recovery during extraction. The normalized for each of the species was then divided by the amount of organic phosphate measured in each of the biological samples. The other mass spectrometer parameters are as follows: ESI voltage: +4500V; Dwell time: 40 ms ; DP (De-clustering Potential): 35.0 V; EP: (Entrance Potential): 10.1 V, CE (Collision Energy): 47.0 V; CXP (Collision cell Exit Potential): 11.6 V, Source Temperature : 450 C, Ion Spray Voltage – 4000 V, Curtain Gas : 35.0, GS1: 15, GS2: 16. The area under the peaks was extracted using MultiQuant v1.1 software (ABSCIEX). Numerical analysis was done in Microsoft Excel.

	Sample					
	Drosophila Larvae			S2R+ cells		
	PIP3 species	Parent Ion	Daughter Ion	PIP3 species	Parent Ion	Daughter Ion
MRM Transitions	32_1	1145.5	547.5	30_1	1119.5	521.5
	32_2	1177.5	579.5	32_0	1149.5	551.5
	34_1	1175.5	577.5	32_1	1147.5	549.5
	34_2	1173.5	575.5	32_2	1145.5	547.5
	34_3	1171.5	573.5	34_0	1177.5	579.5
	36_1	1203.5	605.5	34_1	1175.5	577.5
	36_2	1201.5	603.5	34_2	1173.5	575.5
	36_3	1199.5	601.5	34_3	1171.5	573.5
	36_4	1197.5	599.5	34_4	1169.5	571.5
				34_5	1167.5	569.5
				36_2	1201.5	603.5
				36_3	1199.5	601.5
				36_4	1197.5	599.5
				36_5	1195.5	597.5
				38_3	1227.5	629.5
				38_4	1225.5	627.5
				38_5	1223.5	625.5
				37_4 ISD	1211.5	613.5

Total Organic Phosphate measurement–

1 ml of the organic phase from each sample was taken into phosphate-free tubes and dried completely at 90°C. The remaining steps were performed as described in *Thakur et.al., 2016*.

Preparation of S2R+ cell lysate for *in vitro* PI5P 4- kinase assay

The S2R+ cells were pelleted at 1000g for 10 min and washed with ice-cold PBS Twice. Cells were thereafter homogenized in lysis buffer containing 50mM Tris-Cl, pH – 7.5, 1mM EDTA, 1mM EGTA, 1% Triton-X-100, 50mM NaF, 0.27 M Sucrose, 0.1% β- Mercaptoethanol and freshly added protease and phosphatase inhibitors (Roche). The lysate was then centrifuged at 1000g for 15 min at 4 °C. Protein estimation was performed using the Bradford reagent according to the manufacturer's instructions.

PI5P4-kinase Assay

Vacuum-dried substrate lipid (6 µM PI5P) and 20 µM of phosphatidylserine were resuspended in 10 mM Tris pH 7.4 and micelles were formed by sonication for 2 min in a bath-sonicator. 50 µl of 2× PIPkinase reaction buffer (100 mM Tris pH 7.4, 20 mM $MgCl_2$, 140 mM KCl, and 2 mM EGTA) containing 20 µM ATP, 5 µCi [γ-^{32}P] ATP and cell lysates containing ~10 µg total protein was added to the micelles. The reaction mixture was incubated at 30 °C for 16 h. Lipids were extracted and resolved by one dimensional TLC (45:35:8:2 chloroform: methanol: water: 25% ammonia). The resolved lipids were imaged using phosphorImager.

Western Blotting –

For larval western blots, lysates were prepared by homogenizing 3 wandering third instar larvae or 5 pairs of salivary glands from third instar larvae. In the case of CHO-IR cells, pelleted cells were lysed by repeated pipetting in lysis buffer (same as described above). Thereafter, the samples were heated at 95°C with Laemli loading buffer for 5 min and loaded onto an SDS- Polyacrylamide gel. The proteins were subsequently transferred onto a nitrocellulose membrane and incubated with indicated antibodies overnight at 4°C (for actin/tubulin incubation was done at room temperature for 3 hrs.). Primary antibody concentrations used were – anti- α-actin (SIGMA A5060) 1:1000; anti- dPIP4K 1:1000, anti – GAPDH (Novus Biologicals, #IM-5143A), anti-PIP4KB (Cell Signaling, #9694), anti – pAKTT308 (Cell Signaling, #9275), anti-AKT (Cell Signaling, # 9272). The blots were then washed thrice with Tris Buffer Saline containing 0.1% Tween-20 (0.1% TBS-T) and incubated with 1:10000 concentration of

676 appropriate HRP-conjugated secondary antibodies (Jackson Laboratories, Inc.) for 1.5 hrs. After three
677 washes with 0.1% TBS-T, blots were developed using Clarity Western ECL substrate on a GE
678 ImageQuant LAS 4000 system.

679

680 ## Acknowledgements

681 This work was supported by the National Centre for Biological Sciences, TIFR, Department of
682 Biotechnology, Ministry of Science and Technology (India); and a Wellcome Trust-DBT India Alliance
683 Senior Fellowship to PR. S.S is a recipient of the S.P Mukherji Fellowship from CSIR and S.M an ICMR
684 Fellowship. We thank the NCBS *Drosophila*, Imaging and Lipidomics Facility for support.

685

686 ## References

687 Balakrishnan, S.S., Basu, U., and Raghu, P. (2015). Phosphoinositide signalling in Drosophila. Biochim.
688 Biophys. Acta - Mol. Cell Biol. Lipids *1851*, 770–784.

689 Barbieri, M., Bonafe, M., Franceschi, C., Paolisso, G., Bonafè, M., Franceschi, C., and Paolisso, G. (2003).
690 Insulin/IGF-I-signaling pathway: an evolutionarily conserved mechanism of longevity from yeast to
691 humans. Am J Physiol Endocrinol Metab *285*, 1064–1071.

692 Bohni, R., Riesgo-Escovar, J., Oldham, S., Brogiolo, W., Stocker, H., Andruss, B.F., Beckingham, K., and
693 Hafen, E. (1999). Autonomous control of cell and organ size by CHICO, a Drosophila homolog of
694 vertebrate IRS1-4. *97*, 865–875.

695 Britton, J.S., Lockwood, W.K., Li, L., Cohen, S.M., and Edgar, B.A. (2002). Drosophila's insulin/PI3-
696 kinase pathway coordinates cellular metabolism with nutritional conditions. *2*, 239–249.

697 Brogiolo, W., Stocker, H., Ikeya, T., Rintelen, F., Fernandez, R., and Hafen, E. (2001). An evolutionarily
698 conserved function of the Drosophila insulin receptor and insulin-like peptides in growth control. Curr.
699 Biol. *11*, 213–221.

700 Bulley, S.J., Droubi, A., Clarke, J.H., Anderson, K.E., Stephens, L.R., Hawkins, P.T., and Irvine, R.F.
701 (2016). In B cells, phosphatidylinositol 5-phosphate 4-kinase-α synthesizes $PI(4,5)P_2$ to impact
702 mTORC2 and Akt signaling. Proc. Natl. Acad. Sci. *113*, 10571–10576.

703 Carricaburu, V., Lamia, K.A., Lo, E., Favereaux, L., Payrastre, B., Cantley, L.C., and Rameh, L.E. (2003).
704 The phosphatidylinositol (PI)-5-phosphate 4-kinase type II enzyme controls insulin signaling by
705 regulating PI-3,4,5-trisphosphate degradation. Proc. Natl. Acad. Sci. *100*, 9867–9872.

706 Church, R.B., and Robertson, F.W. (1966). Biochemical analysis of genetic differences in the growth of
707 Drosophila. *7*, 383–407.

708 Clark, J., Anderson, K.E., Juvin, V., Smith, T.S., Karpe, F., Wakelam, M.J.O., Stephens, L.R., and
709 Hawkins, P.T. (2011). Quantification of PtdInsP3 molecular species in cells and tissues by mass

spectrometry. Nat. Methods *8*, 267–272.

Clarke, J.H., Wang, M., and Irvine, R.F. (2010). Localization, regulation and function of type II phosphatidylinositol 5-phosphate 4-kinases. Adv. Enzyme Regul. *50*, 12–18.

Clément, S., Krause, U., Desmedt, F., Tanti, J.F., Behrends, J., Pesesse, X., Sasaki, T., Penninger, J., Doherty, M., Malaisse, W., et al. (2001). The lipid phosphatase SHIP2 controls insulin sensitivity. Nature *409*, 92–97.

Durán, R. V, and Hall, M.N. (2012). Regulation of TOR by small GTPases. EMBO Rep. *13*, 121–128.

Emerling, B.M., Hurov, J.B., Poulogiannis, G., Tsukazawa, K.S., Choo-Wing, R., Wulf, G.M., Bell, E.L., Shim, H.S., Lamia, K.A., Rameh, L.E., et al. (2013). Depletion of a putatively druggable class of phosphatidylinositol kinases inhibits growth of p53-Null tumors. Cell *155*, 844–857.

Engelman, J.A., Luo, J., and Cantley, L.C. (2006). The evolution of phosphatidylinositol 3-kinases as regulators of growth and metabolism. *7*, 606–619.

Georgiev, P., Okkenhaug, H., Drews, A., Wright, D., Lambert, S., Flick, M., Carta, V., Martel, C., Oberwinkler, J., and Raghu, P. (2010). TRPM channels mediate zinc homeostasis and cellular growth during Drosophila larval development. Cell Metab. *12*, 386–397.

Grainger, D.L., Tavelis, C., Ryan, A.J., and Hinchliffe, K. a (2011). Involvement of phosphatidylinositol 5-phosphate in insulin-stimulated glucose uptake in the L6 myotube model of skeletal muscle. Pflugers Arch. *462*, 723–732.

Gual, P., Le Marchand-Brustel, Y., and Tanti, J.-F. (2005). Positive and negative regulation of insulin signaling through IRS-1 phosphorylation. Biochimie *87*, 99–109.

Gupta, A., Toscano, S., Trivedi, D., Jones, D.R., Mathre, S., Clarke, J.H., Divecha, N., and Raghu, P. (2013). Phosphatidylinositol 5-phosphate 4-kinase (PIP4K) regulates TOR signaling and cell growth during Drosophila development. Proc Natl Acad Sci U S A *110*, 5963–5968.

Harrington, L.S., Findlay, G.M., Gray, A., Tolkacheva, T., Wigfield, S., Rebholz, H., Barnett, J., Leslie, N.R., Cheng, S., Shepherd, P.R., et al. (2004). The TSC1-2 tumor suppressor controls insulin-PI3K signaling via regulation of IRS proteins. J. Cell Biol. *166*, 213–223.

Haruta, T., Uno, T., Kawahara, J., Takano, A., Egawa, K., Sharma, P.M., Olefsky, J.M., and Kobayashi, M. (2000). A Rapamycin-Sensitive Pathway Down-Regulates Insulin Signaling via Phosphorylation and Proteasomal Degradation of Insulin Receptor Substrate-1. Mol. Endocrinol. 783–794.

Hawkins, P.T., and Stephens, L.R. (2015). PI3K signalling in inflammation. Biochim. Biophys. Acta - Mol. Cell Biol. Lipids *1851*, 882–897.

Hawkins, P.T., Anderson, K.E., Davidson, K., and Stephens, L.R. (2006). Signalling through Class I PI3Ks in mammalian cells. Biochem. Soc. Trans. *34*, 647–662.

Jones, D.R., Foulger, R., Keune, W.-J., Bultsma, Y., and Divecha, N. (2013). PtdIns5P is an oxidative stress-induced second messenger that regulates PKB activation. FASEB J. *27*, 1644–1656.

Kaisaki, P.J., Delépine, M., Woon, P.Y., Sebag-Montefiore, L., Wilder, S.P., Menzel, S., Vionnet, N.,

746 Marion, E., Riveline, J.-P., Charpentier, G., et al. (2004). Polymorphisms in type II SH2 domain-
747 containing inositol 5-phosphatase (INPPL1, SHIP2) are associated with physiological abnormalities of
748 the metabolic syndrome. Diabetes *53*, 1900–1904.

749 Kockel, L., Kerr, K.S., Melnick, M., Brückner, K., Hebrok, M., and Perrimon, N. (2010). Dynamic switch
750 of negative feedback regulation in Drosophila Akt-TOR signaling. PLoS Genet. *6*, 1–17.

751 Kolay, S., Basu, U., and Raghu, P. (2016). Control of diverse subcellular processes by a single multi-
752 functional lipid phosphatidylinositol 4,5-bisphosphate [PI(4,5)P2]. Biochem. J. *473*, 1681–1692.

753 Lamia, K.A., Peroni, O.D., Kim, Y.B., Rameh, L.E., Kahn, B.B., and Cantley, L.C. (2004). Increased
754 insulin sensitivity and reduced adiposity in phosphatidylinositol 5-phosphate 4-kinase beta-/- mice. Mol
755 Cell Biol *24*, 5080–5087.

756 Lizcano, J.M., Alrubaie, S., Kieloch, A., Deak, M., Leevers, S.J., and Alessi, D.R. (2003). Insulin-induced
757 Drosophila S6 kinase activation requires phosphoinositide 3-kinase and protein kinase B. Biochem. J.
758 *374*, 297–306.

759 Luo, J., Manning, B.D., and Cantley, L.C. (2003). Targeting the PI3K-Akt pathway in human cancer:
760 rationale and promise. Cancer Cell *4*, 257–262.

761 Mackey, A.M., Sarkes, D.A., Bettencourt, I., Asara, J.M., and Rameh, L.E. (2014). PIP4k is a substrate for
762 mTORC1 that maintains basal mTORC1 signaling during starvation. Sci. Signal. *7*, ra104-ra104.

763 Malek, M., Kielkowska, A., Chessa, T., Anderson, K.E., Barneda, D., Pir, P., Nakanishi, H., Eguchi, S.,
764 Koizumi, A., Sasaki, J., et al. (2017). PTEN Regulates PI(3,4)P2Signaling Downstream of Class I PI3K.
765 Mol. Cell *68*, 566–580.e10.

766 McConnachie, G., Pass, I., Walker, S.M., and Downes, C.P. (2003). Interfacial kinetic analysis of the
767 tumour suppressor phosphatase, PTEN: evidence for activation by anionic phospholipids. Biochem. J.
768 *371*, 947–955.

769 Musselman, L.P., Fink, J.L., Narzinski, K., Ramachandran, P.V., Hathiramani, S.S., Cagan, R.L., and
770 Baranski, T.J. (2011). A high-sugar diet produces obesity and insulin resistance in wild-type Drosophila.
771 Dis. Model. Mech. *4*, 842–849.

772 Nässel, D.R., and Broeck, J. Vanden (2016). Insulin/IGF signaling in Drosophila and other insects:
773 factors that regulate production, release and post-release action of the insulin-like peptides. Cell. Mol.
774 Life Sci. *73*, 271–290.

775 Paradis, S., Ailion, M., Toker, A., Thomas, J.H., and Ruvkun, G. (1999). A PDK1 homolog is necessary
776 and sufficient to transduce AGE-1 PI3 kinase signals that regulate diapause in Caenorhabditis elegans.
777 Genes Dev. *13*, 1438–1452.

778 Pasco, M.Y., and Léopold, P. (2012). High sugar-induced insulin resistance in Drosophila relies on the
779 Lipocalin Neural Lazarillo. PLoS One *7*, 1–8.

780 Pesesse, X., Moreau, C., Drayer, A.L., Woscholski, R., Parker, P., and Erneux, C. (1998). The SH2 domain
781 containing inositol 5-phosphatase SHIP2 displays phosphatidylinositol 3,4,5-trisphosphate and inositol
782 1,3,4,5-tetrakisphosphate 5-phosphatase activity. FEBS Lett. *437*, 301–303.

Rameh, L.E., Tolias, K.F., Duckworth, B.C., and Cantley, L.C. (1997). A new pathway for synthesis of phosphatidylinositol-4,5-bisphosphate. Nature *390*, 192–196.

Reilly, K.E.O., Rojo, F., She, Q., Solit, D., Mills, G.B., Lane, H., Hofmann, F., Hicklin, D.J., and Ludwig, D.L. (2011). mTOR Inhibition Induces Upstream Receptor Tyrosine Kinase Signaling and Activates Akt. Cancer Res. *66*, 1500–1508.

Rintelen, F., Stocker, H., Thomas, G., and Hafen, E. (2001). PDK1 regulates growth through Akt and S6K in Drosophila. Proc. Natl. Acad. Sci. U. S. A. *98*, 15020–15025.

Sarkes, D., and Rameh, L.E. (2010). A novel HPLC-based approach makes possible the spatial characterization of cellular PtdIns5P and other phosphoinositides. Biochem. J. *428*, 375–384.

Shah, O.J., Wang, Z., and Hunter, T. (2004). Inappropriate Activation of the TSC/Rheb/mTOR/S6K Cassette Induces IRS1/2 Depletion, Insulin Resistance, and Cell Survival Deficiencies. Curr. Biol. *14*, 1650–1656.

Shim, H., Wu, C., Ramsamooj, S., Bosch, K.N., Chen, Z., Emerling, B.M., Yun, J., Liu, H., Choo-Wing, R., Yang, Z., et al. (2016). Deletion of the gene *Pip4k2c* , a novel phosphatidylinositol kinase, results in hyperactivation of the immune system. Proc. Natl. Acad. Sci. *113*, 7596–7601.

Shingleton, A.W., Das, J., Vinicius, L., and Stern, D.L. (2005). The temporal requirements for insulin signaling during development in Drosophila. PLoS Biol. *3*, e289.

Stephens, L.R., Hughes, K.T., and Irvine, R.F. (1991). Pathway of phosphatidylinositol(3,4,5)-trisphosphate synthesis in activated neutrophils. Nature *351*, 33–39.

Tee, A.R., Manning, B.D., Roux, P.P., Cantley, L.C., and Blenis, J. (2003). Tuberous sclerosis complex gene products, Tuberin and Hamartin, control mTOR signaling by acting as a GTPase-activating protein complex toward Rheb. Curr. Biol. *13*, 1259–1268.

Tremblay, F., Brûlé, S., Hee Um, S., Li, Y., Masuda, K., Roden, M., Sun, X.J., Krebs, M., Polakiewicz, R.D., Thomas, G., et al. (2007). Identification of IRS-1 Ser-1101 as a target of S6K1 in nutrient- and obesity-induced insulin resistance. Proc. Natl. Acad. Sci. U. S. A. *104*, 14056–14061.

Tzatsos, A., and Kandror, K. V (2006). Nutrients suppress phosphatidylinositol 3-kinase/Akt signaling via raptor-dependent mTOR-mediated insulin receptor substrate 1 phosphorylation. Mol. Cell. Biol. *26*, 63–76.

Um, S.H., Frigerio, F., Watanabe, M., Picard, F., Joaquin, M., Sticker, M., Fumagalli, S., Allegrini, P.R., Kozma, S.C., Auwerx, J., et al. (2004). Absence of S6K1 protects against age- and diet-induced obesity while enhancing insulin sensitivity. Nature *431*, 200–205.

Wullschleger, S., Loewith, R., and Hall, M.N. (2006). TOR signaling in growth and metabolism. Cell *124*, 471–484.

Zhang, Y., Gao, X., Saucedo, L.J., Ru, B., Edgar, B. a, and Pan, D. (2003). Rheb is a direct target of the tuberous sclerosis tumour suppressor proteins. Nat. Cell Biol. *5*, 578–581.

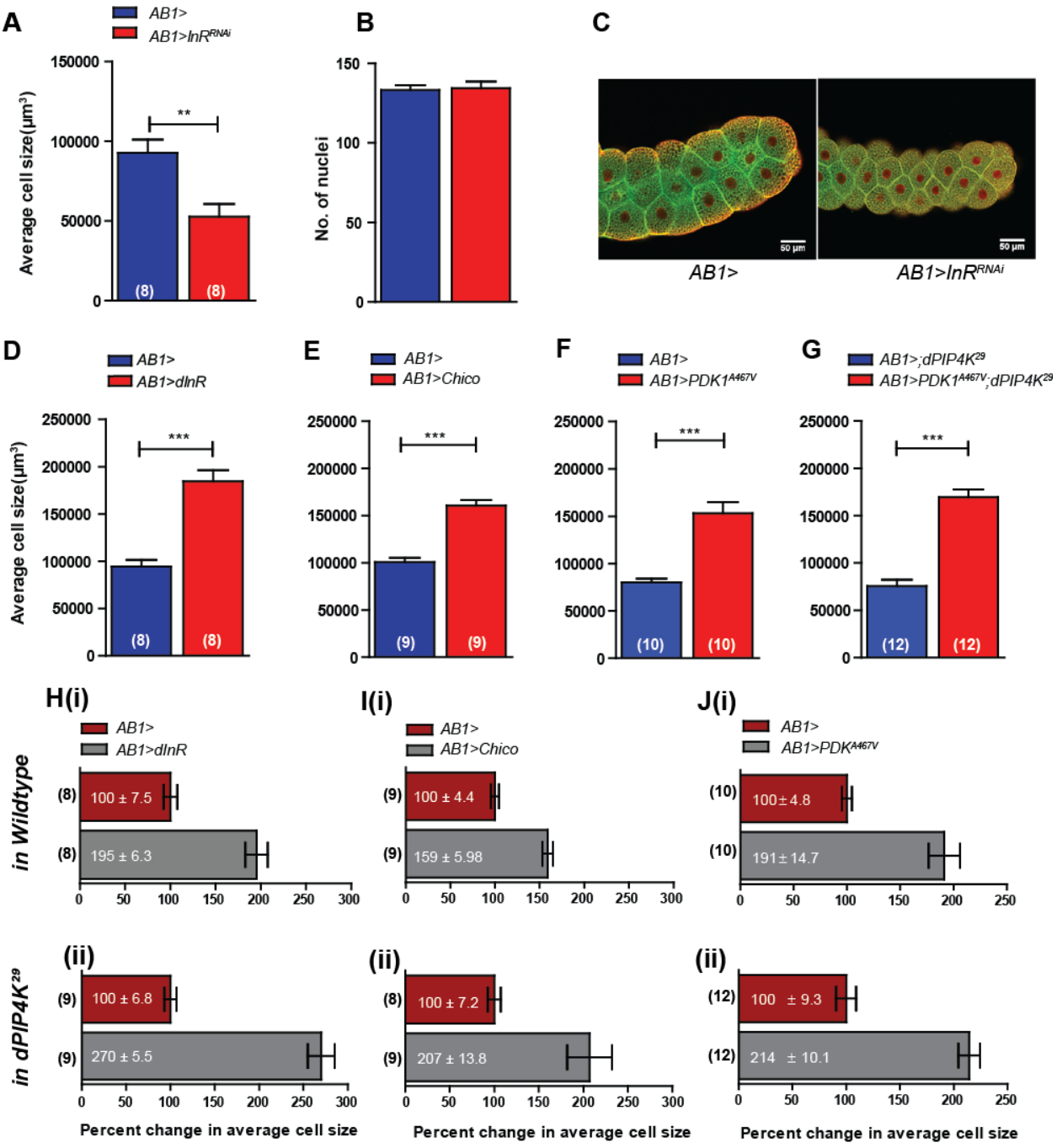

Sharma, et.al. Fig. 1

Fig 1. dPIP4K epistatically interacts with insulin receptor signalling

Cell size measurements upon knockdown of Insulin receptor in salivary glands – **A.** Cell size measurements **B.** Quantification of the no. of nuclei **C.** Representative confocal sections of salivary glands of wandering third instar larvae labelled with green dye labelled BODIPY and TOTO3 to mark the nuclei. Graphs represent mean ± SEM. **D.** Overexpression of insulin receptor (InR) **E.** Overexpression of insulin receptor substrate-Chico **F.** Overexpression of $PDK1^{A467V}$ **G.** Overexpression of $PDK1^{A467V}$ in $dPIP4K^{29}$. **H-J'.** Comparison of relative changes in cell size upon overexpression InR, chico and $PDK1^{A467V}$ in *wildtype* (**H(i), I(i), J(i)**) and $dPIP4K^{29}$ (**H(ii), I(ii), J(ii)**) salivary glands respectively. Scale: 50 μm. Graphs represent mean ± SE normalized to the mean of the ctrl. On each graph, numbers inside the parentheses indicate the no. of biological replicates used for the measurement. *Student's t-test* used for statistical analysis. $^{**}p\text{-value} < 0.01$, $^{***}p\text{-value} < 0.001$.

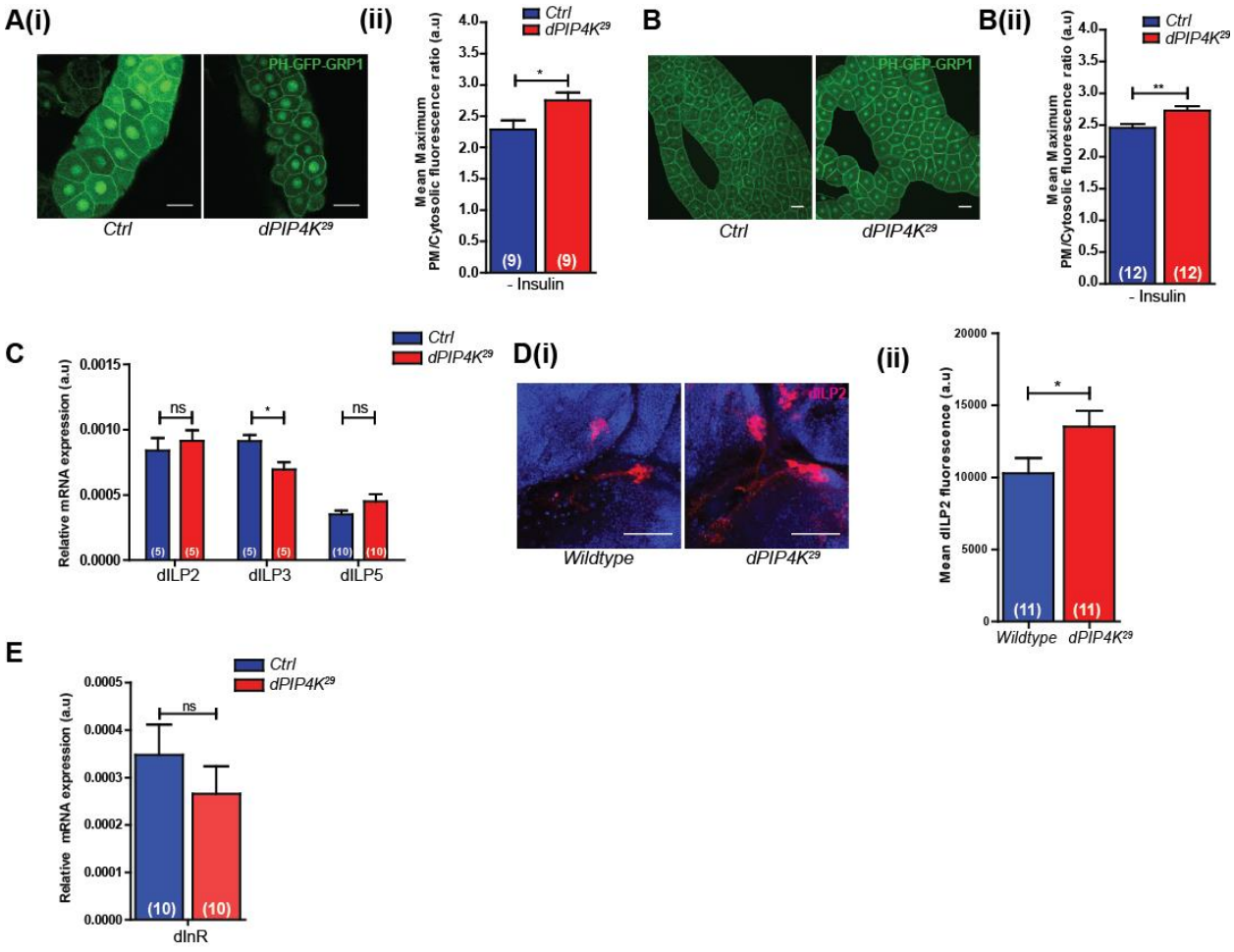

Sharma, et.al. Fig. 2

Fig 2. Plasma membrane PIP_3 levels are elevated in *dPIP4K* mutant tissues without an increase in humoral dILP secretion

A-B'. PIP_3 quantification – Images showing the intensity and localization of the PIP_3 binding probe (GFP-PH-GRP1) in larval tissues. The PIP_3 levels were quantified as the ratio of the probe fluorescence intensity on the plasma membrane to that in the cytosol. **A(i).** Representative confocal images showing the distribution of the probe in the salivary glands. **A(ii).** Quantification of PIP_3 levels between control and $dPIP4K^{29}$ salivary glands for experiment depicted in A(i). (Data represents mean of fluorescence intensity ratios calculated from a minimum of 10 cells from each salivary gland). **B(i).** Representative confocal images showing the distribution of the probe in the fat body and in **B(ii)** the quantification from these experiments. The ratio was calculated from about 50 cells from 12 fat body regions pooled from 5 animals for each genotype respectively. Wandering third instar larvae used for measurements. Scale: 50 μm for salivary gland images and 10 μm for fat body images **C.** qPCR measurements for mRNA levels of *dILP 2, 3* and *5* from whole larvae. Transcript levels for each gene were normalized to the mRNA levels of *rp49* in the same sample. Graphs represent mean ± SEM **D.** qPCR measurements for *dInR*. Transcript levels for each gene were normalized to the mRNA levels of *rp49* in the same sample **E(i).** Confocal z-projections showing immunostaining for dILP2 in larval IPCs **E(ii).** Quantification showing mean ± SEM of dILP2 staining intensity in the third instar wandering larval brains. On each graph, numbers inside the parentheses indicate the no. of biological replicates used for the measurement. Scale: 50 μm. *Student's t-test* used for statistical analysis. $*p\text{-value} < 0.05$, $**p\text{-value} < 0.01$.

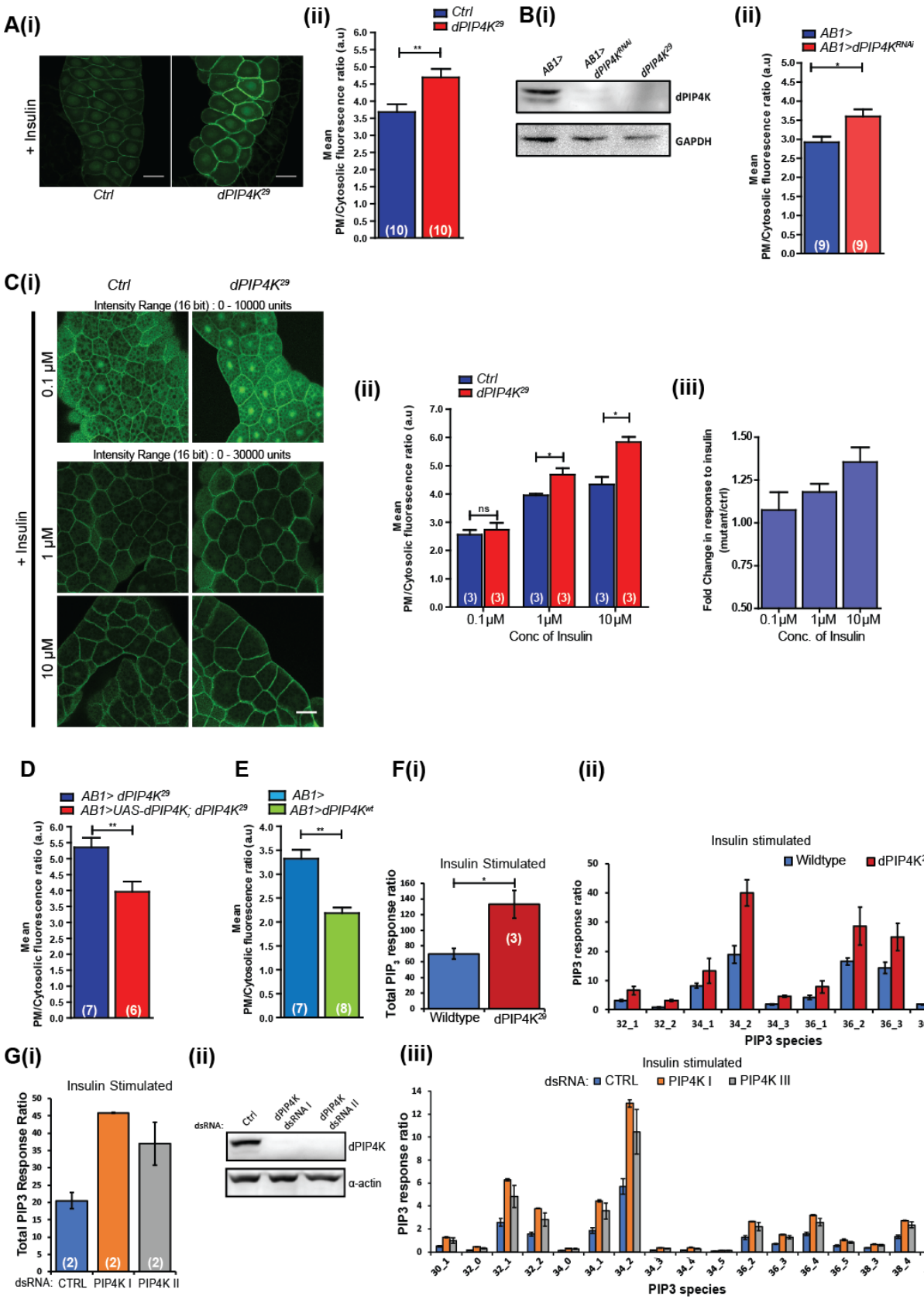

Sharma, et.al. Fig. 3

Fig 3. Increased sensitivity of *Drosophila* larval cells to insulin stimulation upon loss of dPIP4K.

A(i). Confocal z-projections showing levels and localization of the PIP_3 probe in control and *dPIP4K*^{29} in salivary glands cells stimulated with 10 μM insulin for 10 min and in **A(ii)**, quantification of PIP_3 levels between control and *dPIP4K*^{29} salivary glands from the same set of experiments. The graph represents mean ± SEM. **B(i).** Confocal z-projections of fat body lobes expressing PIP_3 binding probe from control and *dPIP4K*^{29} late third instar larvae stimulated with 0.1 μM, 1 μM and 10 μM insulin post 2 hr starvation. **B(ii).** Quantification of PIP_3 for experiments in fig. **B** (50 cells from at least 3 samples in the fat body for each genotype and treatment used for analysis). Scale: 50 μm. **B(iii).** Comparison of mean fold change (mutant w.r.t control) in response to insulin computed from data in B'. Error bars indicate SEM. **C(i).** Immunoblot (from wandering third instar stage) showing a reduction in levels of dPIP4K protein in salivary gland lysates upon knockdown of dPIP4K using *AB1*GAL4. Relative quantification of PIP_3 levels using the GFP-PH-GRP1 probe between, (**C(ii)**) control and *dPIP4K*-knockdown salivary glands (**D**) mutant and rescue salivary glands and (**E**) wildtype and salivary glands overexpressing dPIP4K. Graphs show mean PIP_3 levels ± SEM. Scale: 50 μM. **F(i).** Measurement of total PIP_3 levels in whole larval lipid extracts from wildtype and *dPIP4K*^{29} using LCMS. **F(ii).** Levels of various larval PIP_3 species in wildtype and *dPIP4K*^{29} whole larval lipid extracts. **G(i).** Measurement of total PIP_3 levels using LCMS in whole cell lipid extracts from S2R+ cells treated with indicated dsRNAs. **F(ii).** Levels of various larval PIP_3 species in whole cell lipid extracts from S2R+ cells. The graphs show mean PIP_3 levels (normalized to spiked internal standards and total lipid phosphates recovered). Error bars depict SEM. *Student's t-test* used for statistical analysis. **p-value* < 0.05, ***p-value* <0.01. On each graph, numbers inside the parentheses indicate the no. of biological replicates used for the measurement.

A

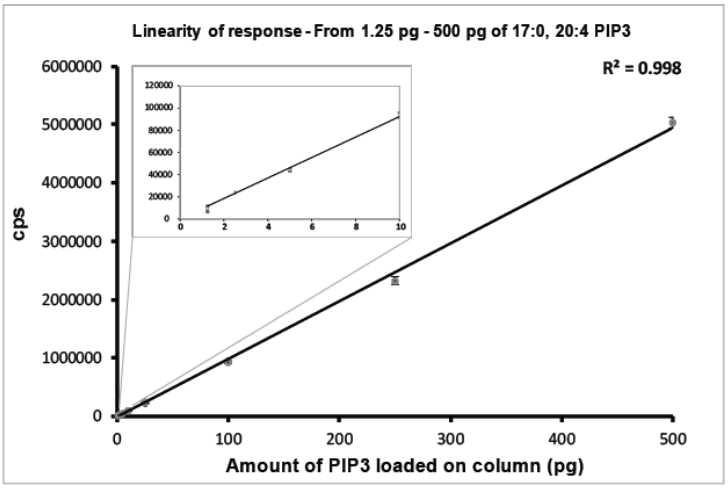

B

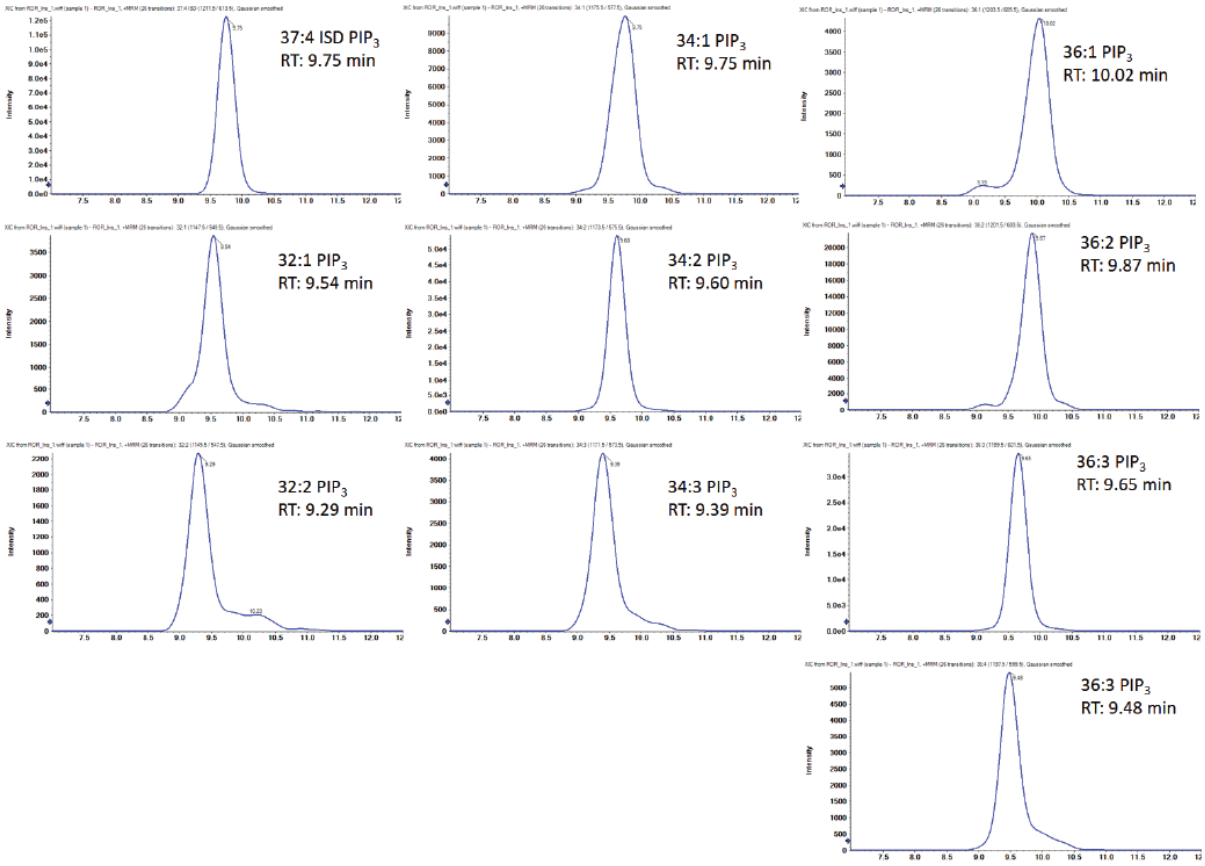

Sharma, et.al. Fig. 3, Supplement 1

Fig. 3, Supplement 1.

(i) Linearity of mass spectrometer response for increasing amounts of PIP_3 standard (17:0, 20:4) injected. Each point on the curve indicates the mean ± SD of three replicate injections. (ii) Chromatograms showing the elution profiles and retention times for various PIP_3 species detected from whole larval lipid extracts of wildtype larvae stimulated *ex-vivo* with 100 µM insulin for 10 min. Note the changing retention times with increase in no. of double bonds and increase in length of acyl chains. Increase in double bonds for a fixed acyl chain length results in earlier elution. Increase in length of acyl chain delays elution.

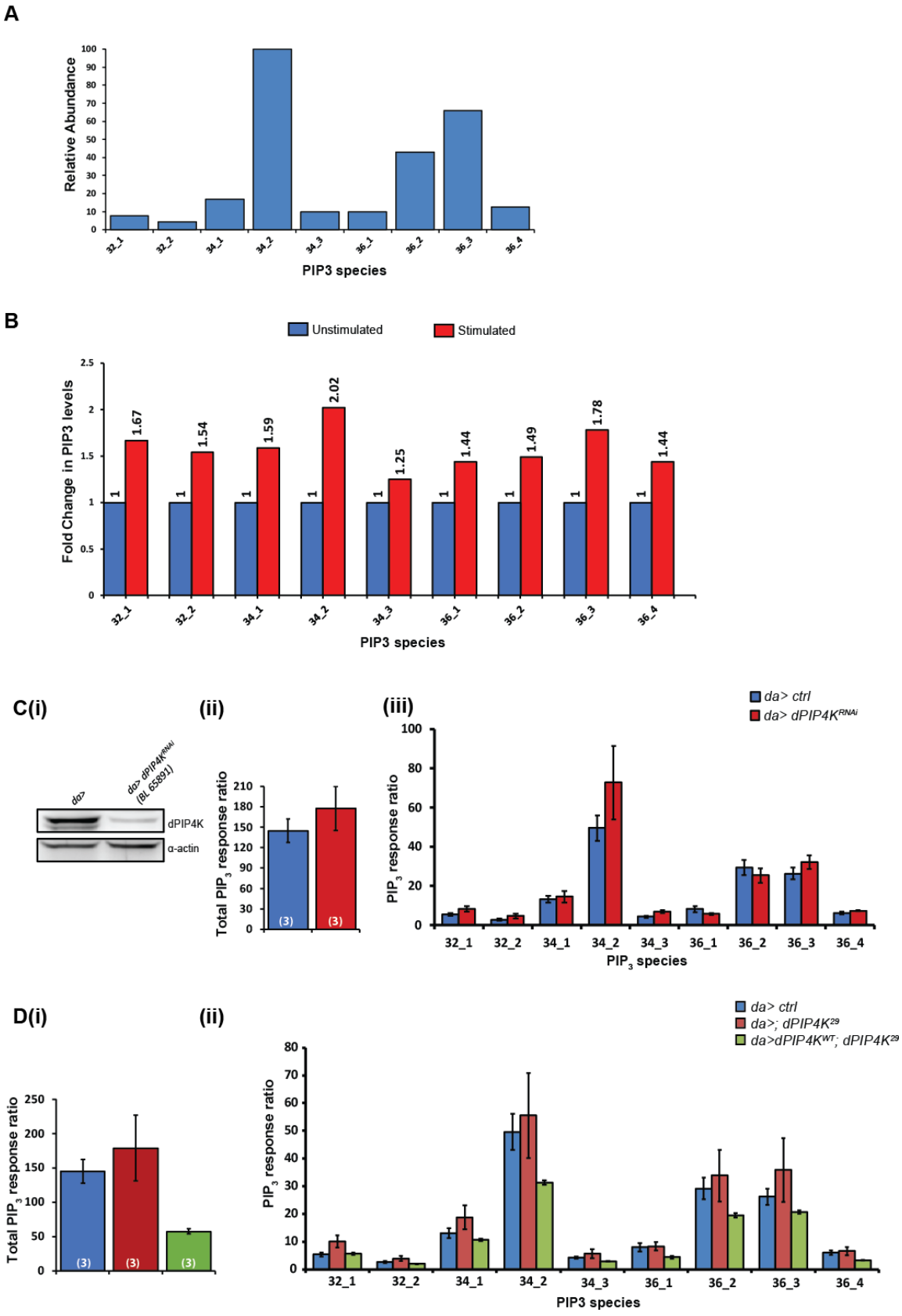

Sharma, et.al. Fig. 3, Supplement 2

Fig. 3, Supplement 2.

Quantitative measurement of total PIP_3 levels and individual PIP_3 species from whole larval lipid extracts of wandering third instar larvae. **A.** Relative abundance of various PIP_3 species in whole larval lipid extracts of wildtype larvae stimulated *ex-vivo* with 100 μM insulin for 10 min. **B.** A control experiment showing changes in the levels of various PIP_3 species upon insulin stimulation (100 μM, 10 min). **C(i).** Immunoblot from whole larval lysates showing reduction in levels of dPIP4K protein upon pan-larval RNAi for dPIP4K using *da*GAL4. **C(ii).** Total levels of PIP_3 in whole larval control and $dPIP4K^{RNAi}$ lipid extracts **C(iii).** Levels of various larval PIP_3 species in whole larval control and $dPIP4K^{RNAi}$ lipid extracts. Total PIP_3 levels (**D(i)**) and levels of individual species (**D(ii)**) in whole larval GAL4-control (*da>*), GAL4-control in $dPIP4K^{29}$ background (*da>; dPIP4K*^{29}) and pan-larval rescue (*da>dPIP4K; dPIP4K*^{29}) lipid extracts. The graphs show mean PIP_3 levels (normalized to spiked internal standards and total lipid phosphates recovered). Error bars depict SEM. On each panel, numbers inside the parentheses indicate the no. of biological replicates used for the measurement.

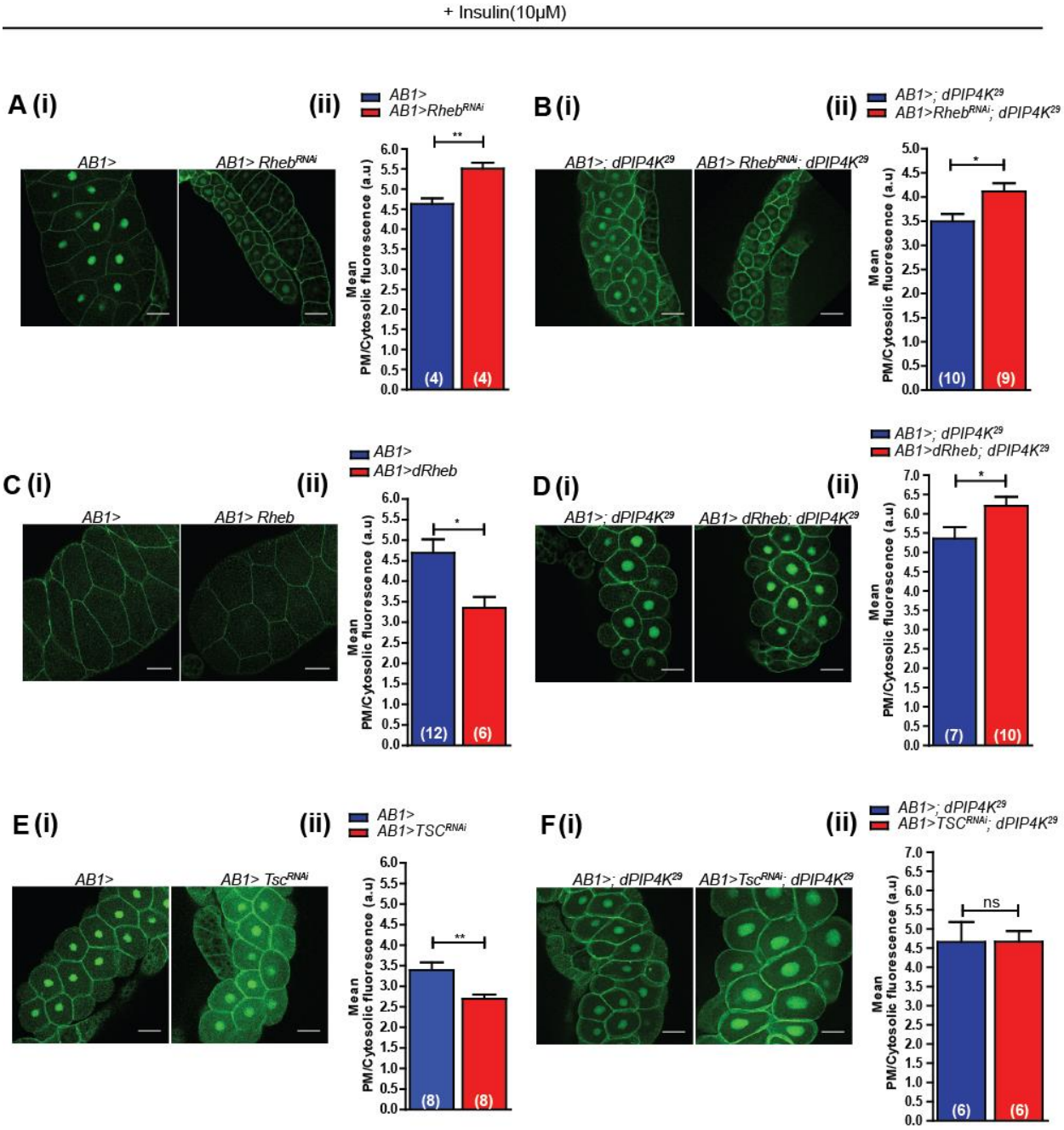

Sharma, et.al. Fig. 4

Fig 4. Reduced TORC1-mediated negative feedback regulation of insulin signalling in *dPIP4K*^{29}cells.

PIP_3 quantification – Salivary gland images showing the distribution of the PIP_3 binding probe GFP-PH-GRP1 in cells. The distribution was quantified as the ratio of probe fluorescence on the plasma membrane to that in the cytosol. Data represent mean of fluorescence ratios (indicative of PIP3 levels). In all these experiments, the genetic manipulation was restricted to the salivary glands using *AB1*Gal4 **A-C.** In a wildtype background, Downregulation of TOR signalling by RNAi for *Rheb* [**A (i and ii)**]. Upregulation of TOR signalling through overexpression of *Rheb* [**B (i and ii)**], knockdown of *Tsc* [**C (i and ii)**] **D-F.** In a *dPIP4K*^{29} background, Downregulation of TOR signalling by RNAi for *Rheb* [D **(i and ii)**]Upregulation of TOR signalling through overexpression of Rheb [**E (i and ii)**], knockdown of Tsc [**F (i and ii)**]. Graphs represent mean ± SEM. *Student's t-test* used for statistical analysis. **p-value* < 0.05. ***p-value* <0.01. On each graph, numbers inside the parentheses indicate the no. of biological replicates used for the measurement.

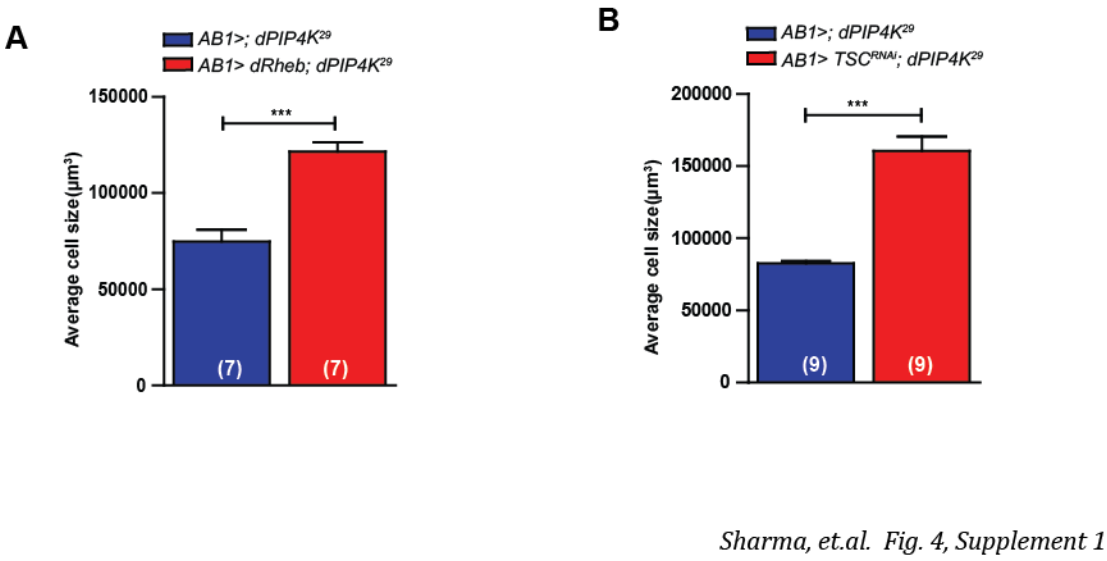

Sharma, et.al. Fig. 4, Supplement 1

Fig. 4, Supplement 1

Cell size measurements in salivary glands of *dPIP4K*^{29} upon (A) overexpression of dRheb (B) Knockdown of TSC. Graphs represent mean ± SEM. On each panel, numbers inside the parentheses indicate the no. of biological replicates used for the measurement.

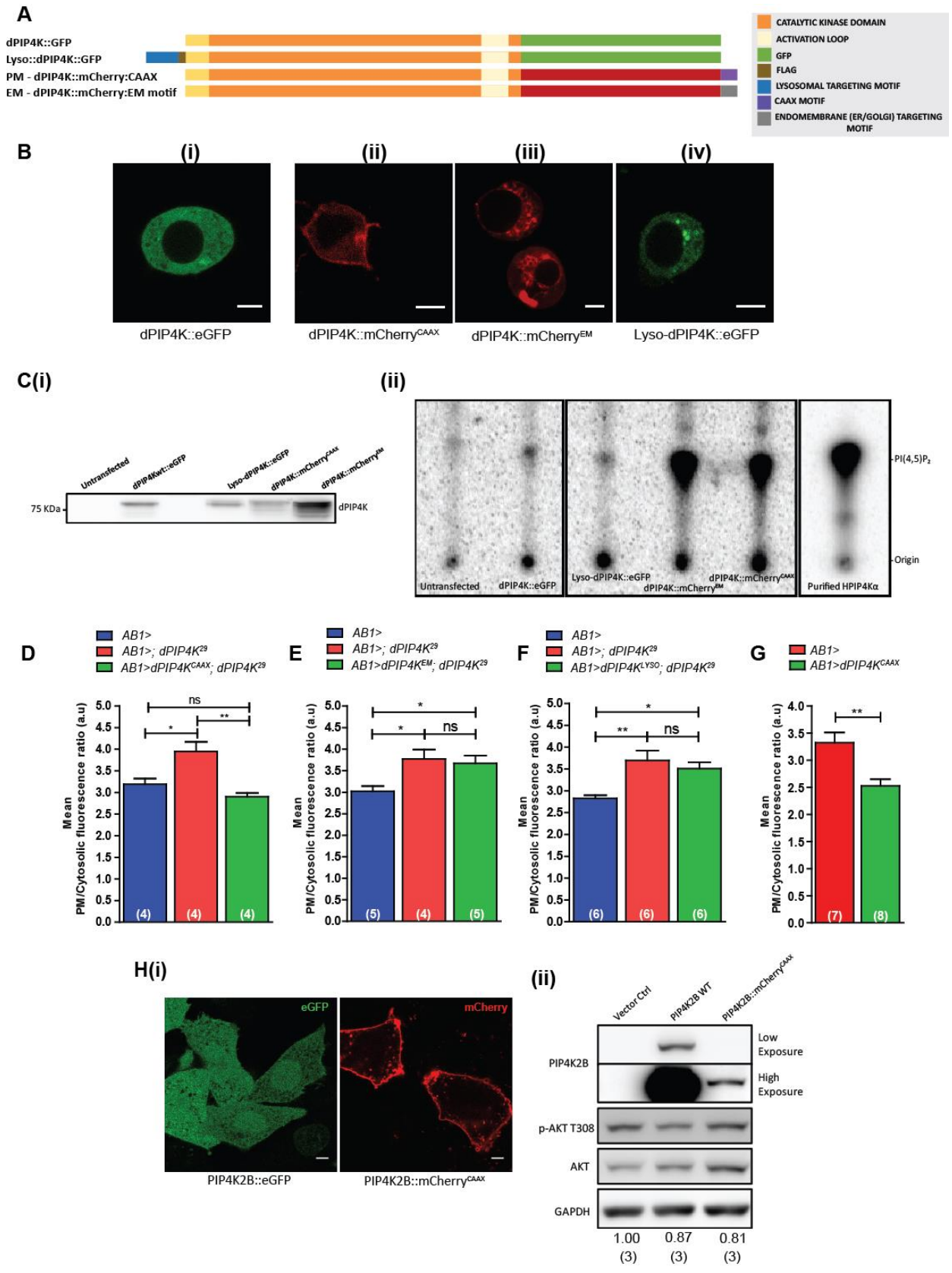

Sharma, et.al. Fig. 5

Fig 5. PIP4K functions at the plasma membrane as a negative regulator of insulin receptor signalling

A. Schematic showing constructs that target dPIP4K to different subcellular compartments and the motifs used for targeting. **B (i-iv).** Representative confocal z-projections of S2R+ cells with act-GAL4 expressing various dPIP4K constructs **(i)** wildtype GFP-tagged dPIP4K **(ii)** plasma-membrane (PM) targeted mCherry-tagged dPIP4K **(iii)** mCherry tagged dPIP4K targeted to various intracellular membranes inclusive of ER, Golgi and endo-lysosomal system **(iv)** GFP-tagged dPIP4K targeted to the lysosome. **C(i).** Immunoblots from S2R+ lysates showing the expression of indicated dPIP4K constructs that were used in the *in vitro* assay. **C(ii).** *In vitro* kinase assay from S2R+ cell lysates showing the activity of different overexpressed dPIP4K constructs. PIP_3 measurement on insulin stimulation (10 μM) using the PH-GFP-GRP1 probe **D-F.** in *dPIP4K*^{29} salivary glands reconstituted with **D.** PM targeted dPIP4K, **E.** endo-membrane targeted dPIP4K, **F.** Lysosomal dPIP4K, **G.** upon overexpression of dPIP4K::mCherry^{CAAX} in the salivary glands. Graphs represent mean ± SEM from at least 4 biological replicates. **H(i).** Representative confocal z-projections of CHO-IR cells overexpressing GFP-PIP4K2B and PIP4K2B::mCherry-CAAX. **H(ii).** Immunoblots from CHO-IR cells expressing PIP4K2B constructs stimulated with 1 μM insulin for 10 min. The values below the blots represent the mean pAKT/Total AKT ratio across three independent experiments. Student's t-test used for statistical analysis. *p-value < 0.05, **p-value < 0.01. On each panel, numbers inside the parentheses indicate the no. of biological replicates used for the measurement.

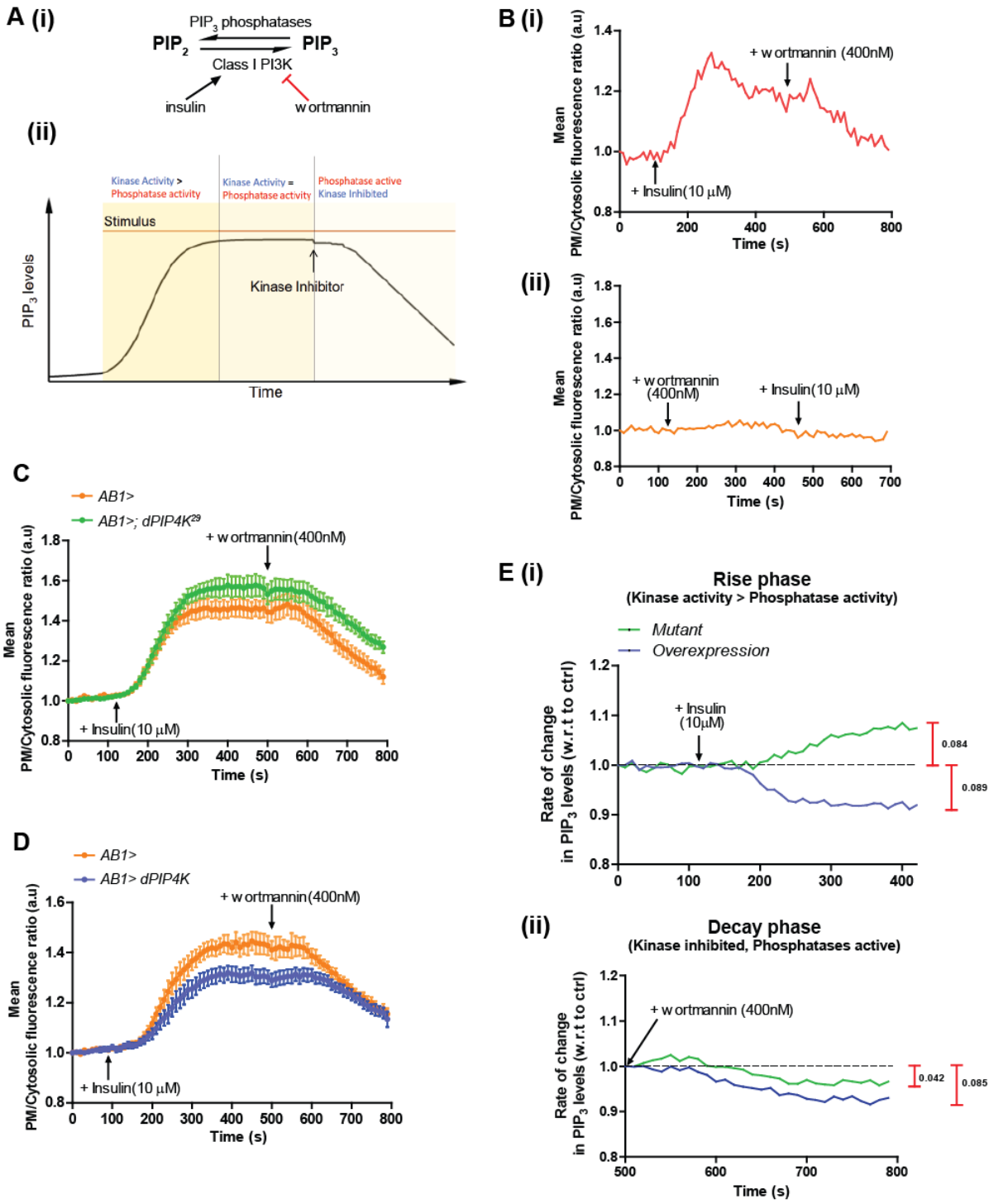

Sharma, et.al. Fig. 6

Fig 6. dPIP4K influences PIP_3 turnover.

(**A(i)**) Schematic of the reactions that determine PIP_3 turnover at the plasma membrane. Insulin stimulates PI3K activation. Wortmannin inhibits PI3K activity irreversibly. (**A(ii)**) Live imaging assay protocol to follow PIP_3 dynamics with three phases as depicted. (**B(i)**) A single trace from live imaging of salivary glands expressing GFP-PH-GRP1 probe showing the changes in the plasma-membrane to cytosolic ratio of the probe fluorescence over time. (**B(ii)**) Wortmannin addition (400nM) completely blocks insulin (10μM) induced PIP_3 production. (**C**) and (**D**) Average traces of GFP-PH-GRP1 fluorescence ratio from multiple imaging runs for the genotypes indicated (N=7 for all genotypes). The two experiments were performed at different times, hence controls samples were repeated. (**E(i) and (ii)**) Curves depict changes in slopes of fluorescence calculated by taking ratios of fluorescence from test genotypes to that in controls. The maximal difference is indicated alongside the graph.

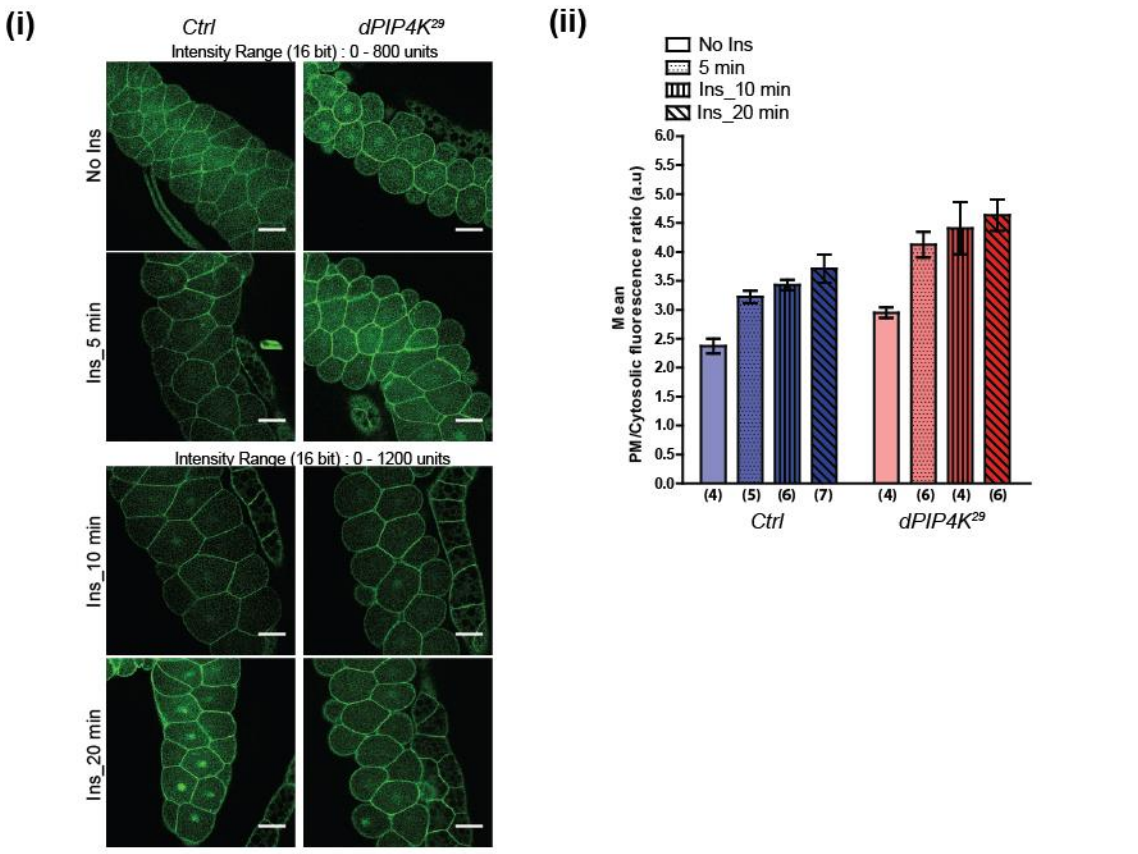

Sharma, et.al. Fig. 6, Supplement 1

Fig. 6, Supplement 1

A. (i) Confocal z-projections of salivary glands expressing GFP-PH-GRP1 in wildtype and *dPIP4K*^{29} backgrounds. Salivary glands dissected from wandering 3 rd instar larvae were stimulated or not with 10 μM bovine insulin for indicated times, fixed and imaged. (ii) Relative PIP_3 levels were measured as a ratio of mean fluorescence intensity at the plasma membrane to that in the cytosol. Graphs represent mean ± SEM. On each panel, numbers inside the parentheses indicate the no. of biological replicates used for the measurement.

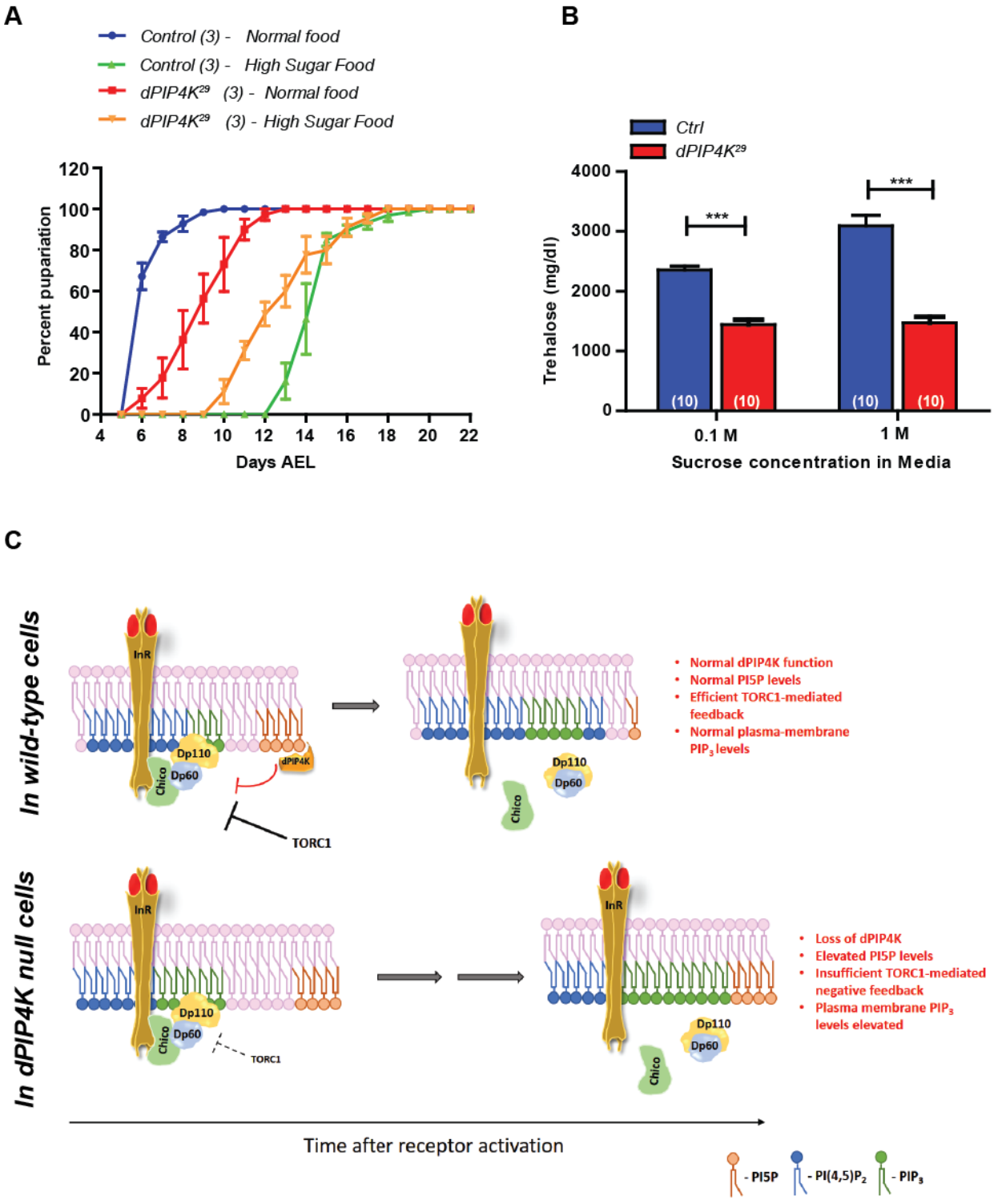

Sharma, et.al. Fig. 7

Fig 7. dPIP4K modulates the acquisition of insulin resistance upon high dietary sugar intake.

A. The graph represents the mean percentage of pupariation (After egg laying, AEL) observed over time on indicated diets. Data collected from 3 independent batches of about 15-25 larvae per batch. Error bars indicate SEM. **B.** Mean hemolymph trehalose levels measured of hemolymph pooled from 5-8 larvae each per genotype. Error bars represent SEM. *Student's t-test* used for statistical analysis. ***p-value* <0.001. On each panel, numbers inside the parentheses indicate the no. of biological replicates used for the measurement. **C.** A schematic of regulation of PIP_3 levels by dPIP4K upon insulin stimulation. In wild-type cells, insulin-induced activation of the receptor triggers dPIP4K activity that prevents PI5P elevation at plasma membrane. Eventually, the negative feedback via TORC1 activity also sets in. These events act together and keep PIP_3 levels in check. Upon loss of dPIP4K in cells, PI5P accumulates and cells show increased PIP_3 levels upon insulin stimulation as a result of increased PI3K activity which cannot be restored via TORC1-mediated negative feedback.